Parametric Demonstration of Load-Dependent Critical Temperatures for Flexural Fire Resistance of Composite W-Shape Floor Beams

MICHAEL M. DRURY and SPENCER E. QUIEL

ABSTRACT

Parametric numerical modeling was performed for three composite floor beam configurations (with different W-shape sections and one-way span lengths supported by shear connections) under exposure to one standard fire and three natural fire temperature-time histories. The parametric matrix included three levels of passive fire protection, four combinations of axial and rotational restraint at the beam ends, and three levels of applied flexural loading. A previously validated lumped mass heat transfer modeling approach was used to calculate steel temperatures for each flange and the web, and a one-dimensional finite element (FE) heat transfer modeling approach was used to calculate the temperature gradient through the structural thickness of the floor slab. A previously validated fiber-beam FE structural modeling approach was then used to model the flexural response of the one-way composite beam under fire. The results of parametric analysis showed that the loss of flexural resistance under any fire exposure can be conservatively predicted using a critical bottom flange temperature based on AISC 360-22, Table A-4.2.4, which is expressed as a function of the applied flexural utilization ratio, M/M_n. The bottom flange temperature at which flexural failure would occur was relatively consistent regardless of variations in beam end restraint as well as the level of applied fire protection. For composite beams that survived natural fire exposure through burnout, the bottom flange temperature always remained below the load-dependent critical value. In those cases, variations in beam end restraint significantly impacted the magnitude of residual tensile reaction forces that develop at the ends of the beam during cooling.

Keywords: composite W-shape floor beam, standard fire resistance, natural fire resilience, critical bottom flange temperature, passive fire protection, spray-applied fire resistive material (SFRM).

INTRODUCTION

Floor systems in steel-framed buildings commonly consist of W-shape filler beams that support a reinforced concrete slab, which is placed on light-gage corrugated metal decking (see Figure 1). The beam and slab are often constructed to be composite via the placement of shear studs at their interface, thereby enhancing their combined flexural stiffness and moment capacity (Vinnakota et al., 1988). The amount of passive fire protection applied to these beams must satisfy the hourly rating requirements of the *International Building Code* (IBC), Table 601 (ICC, 2023). To achieve these ratings in current practice, the W-shape beam is often contour-coated with spray-applied, fire-resistive material (SFRM), a lightweight cementitious product with low thermal diffusivity (UL, 2022a).

Michael M. Drury, Associate, Wiss, Janney, Elstner Associates, Inc., Princeton, N.J. Email: mdrury@wje.com

Spencer E. Quiel, Associate Professor, Department of Civil and Environmental Engineering, Lehigh University, Bethlehem, Pa. Email: seq213@lehigh.edu (corresponding)

Paper No. 2025–04

Hourly ratings represent the time at which a floor beam would be expected to "fail" (by reaching a specified thermal or structural response limit) when subjected to a standard fire exposure (see Figure 2). The initial 2 hr period of a standard fire curve such as ASTM E119 (ASTM, 2024) is intended to generally represent the ramp-up of temperature in a post-flashover building compartment. The fire temperature then increases gradually and indefinitely with no subsequent decay phase nor any consideration of the impact of active fire protection, such as sprinklers. This indefinite continuation of high temperature exposure ensures that the assembly will ultimately reach a targeted response limit when subjected to a standard fire test.

For composite floor beams, hourly ratings provide a standardized metric for flexural fire resistance that enables the selection and comparison of section configurations and passive fire protection materials based on testing. However, an hourly rating does not explicitly quantify the resilience of an assembly when exposed to a realistic or "natural" fire in a building. The temperature-time history for a natural fire exposure is characterized by a rapid initial increase to a fully developed state, followed by eventual "burnout" (i.e., a transition to a decay or cooling phase, as shown in Figure 2). The shape and duration of a natural fire curve depend on the characteristics of the building compartment, including geometry, fuel load, ventilation, and lining materials.

Performance-based structural fire design (PBSFD) evaluates structural response to natural fire, both at the peak response during the fire and (if failure does not occur) in its residual state following burnout and cooling (ASCE, 2020). PBSFD can be implemented per IBC Section 703.2.3 as an alternative method of design under approval of the building official or other authority having jurisdiction (AHJ) (ICC, 2023). Guidance for conducting PBSFD of steel building construction is available in design standards such as ASCE 7-22, Appendix E (ASCE, 2022) and AISC 360-22, Appendix 4 (2022), as well as other references such as the ASCE *Manual of Practice 138* (LaMalva, 2018).

When exposed to fire, flexurally loaded composite beams will thermally weaken and develop additional stress due to axial and rotational restraint of thermal expansion. If the steel beam reaches a "critical" temperature, then the floor

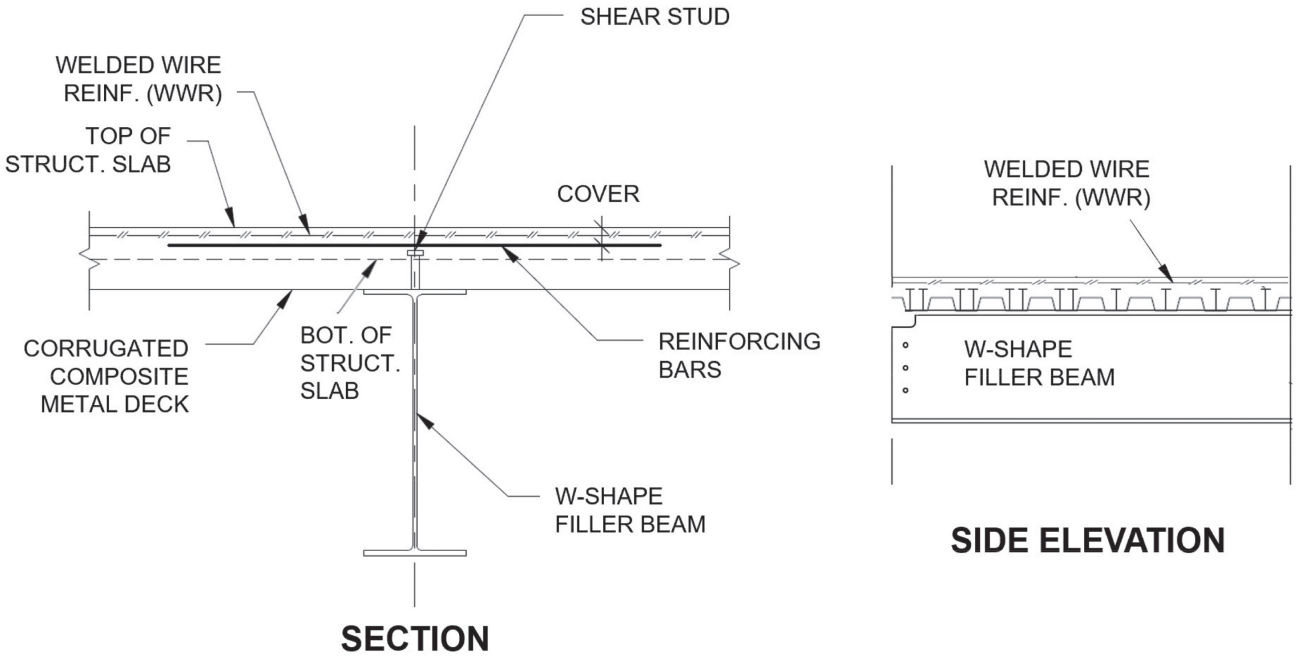

Fig. 1. Representative composite filler floor beam configuration. Side elevation is shown with bolt holes and top flange coping to accommodate a shear connection.

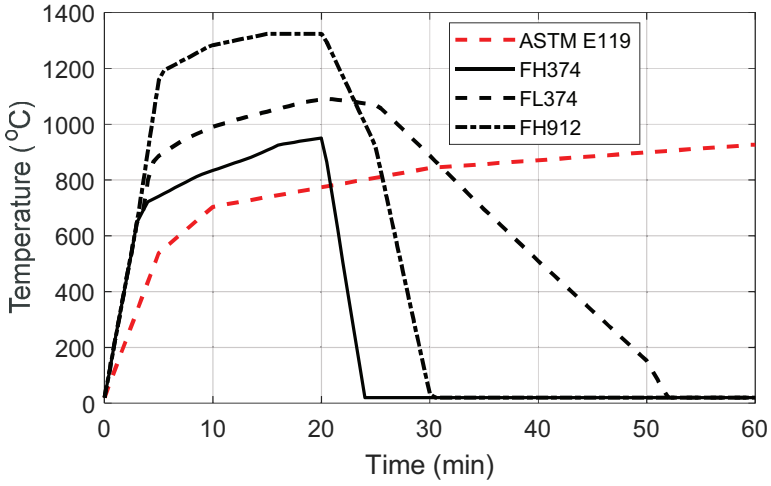

Fig. 2. Representative temperature-time histories of fire exposure: standard fire curve per ASTM E119 (2024) and three natural fire curves from an ASCE exemplar study (2020).

Table 1. Temperature-Dependent Moment Capacity Retention Factors for Composite Floor Beams (Reproduced from AISC 360-22, Table A-4.2.4)	
Moment Capacity Retention $k_{cb} = M_{n,T}/M_n$	**Bottom Flange Temperature $T_{s,BF}$, °F (°C)**
1.00	68 (20)
0.98	300 (150)
0.95	600 (320)
0.89	800 (430)
0.71	1000 (540)
0.49	1200 (650)
0.26	1400 (760)
0.12	1600 (870)
0.02	1800 (980)
0.00	2000 (1100)

system will experience a significant increase in deflection and be at risk of collapse due to the loss of flexural resistance. As would be expected, these critical temperatures are dependent on the level of applied loading, which can be expressed as a ratio of applied moment divided by the initial ambient moment capacity of the composite floor beam cross section. When the floor beam is heated by a fire below, the top flange temperature ($T_{s,TF}$) remains cooler than that of the web and bottom flange ($T_{s,web}$ and $T_{s,BF}$) because the upper surface of the top flange is in contact with the supported floor slab and is thus shielded from direct heating. The values of $T_{s,web}$ and $T_{s,BF}$ are often similar (AISC, 2022; CEN, 2008a), but the response of the bottom flange is more critical to the flexural fire resistance of the composite section (Drury, 2022; Selden, 2014). AISC 360-22, Table A-4.2.4 (2022) provides a moment capacity retention factor ($k_{cb} = M_{n,T}/M_n$) for composite beams as a function of $T_{s,BF}$. Those values (reproduced in Table 1) can be reframed as a function of critical bottom flange temperature, $T_{cr,BF}$, for varying levels of initially applied flexural utilization at ambient conditions, M/M_n (Drury and Quiel, 2025).

In this paper, parametric numerical analyses are used to demonstrate the robustness of the relationship between $T_{cr,BF}$ and M/M_n in Table 1 for one-way composite floor beams with realistic combinations of span length, beam section size, end restraint conditions, and applied SFRM thickness when subjected to either standard or natural fire exposure. By establishing $T_{cr,BF}$ as a consistent indicator of flexural failure under any fire, the hourly rating under standard fire exposure can be determined for a given composite beam and SFRM thickness by calculating the time history of $T_{s,BF}$ via the lumped mass methods presented in Drury and Quiel (2025). In the context of PBSFD, the relationship between $T_{cr,BF}$ and M/M_n in Table 1 can also serve as a threshold below which a composite beam assembly would be expected to survive natural fire exposure through burnout without experiencing flexural runaway. Using load-dependent $T_{cr,BF}$, a designer can thereby correlate an hourly rating for a given composite floor beam configuration to its survivability under a range of natural fire hazards and applied loading.

REVIEW OF PREVIOUS TESTING

Previous work by Drury and Quiel (2025) showed that reframing the relationship in Table 1 as a load-dependent $T_{cr,BF}$ can provide a conservatively accurate prediction of the loss of flexural resistance observed in numerous standard and quasi-standard fire tests (Alfawakhiri et al., 2016; Bletzacker, 1967; Choe et al., 2019, 2020; Drury and Quiel, 2025; Jiang et al., 2017; Kordosky et al., 2020; Wang et al., 2017a; Zhao and Kruppa, 1997) for a wide range of W-shape steel floor beam configurations:

- One-way spans varying from 3.35–12.2 m (11–40 ft).
- Varying section sizes with composite and noncomposite slabs.
- End conditions that are restrained, unrestrained, or partially restrained.
- Connections that range from idealized bearing supports to realistic shear connections.
- Applied loading that induces an initial value of M/M_n ranging from 25–80%.
- Varying levels of contour coated with spray-applied fire resistive material (SFRM), a lightweight cementitious

product with low thermal diffusivity that is commonly used as passive fire protection for W-shape floor beams in current practice).

For illustration, the setups for quasi-standard fire tests per Kordosky et al. (2020) and Choe et al. (2019) are summarized in Table 2. The temperature-time histories applied to each specimen from those programs are plotted in Figure 3. The tests on these W12×26 and W18×35 composite beams are referred to a quasi-standard because their temperature-time histories met or slightly exceeded that of the ASTM E119 standard, and the curves plotted in Figure 3 for these specimens are terminated when they experienced a rapid increase in deflection (i.e., when they approached flexural runaway) and the applied loading was removed. Plots of midspan deflection versus $T_{s,BF}$ in Figure 4 show that the values of $T_{cr,BF}$ for each corresponding M/M_n per Table 1 provide a very good indication of the onset of flexural runaway, regardless of the composite cross-section characteristics, span length, the presence of passive fire protection, and the restraint of the beam ends.

Setups for natural fire tests per Drury et al. (2021) and Drury and Quiel (2023a) are also summarized in Table 2. These tests on W8×10 and W8×28 composite beams were conducted such that the specimens were subjected to the corresponding natural temperature-time histories in Figure 3 and did not experience flexural runaway. Both beams developed significant midspan deflection and restraint reactions

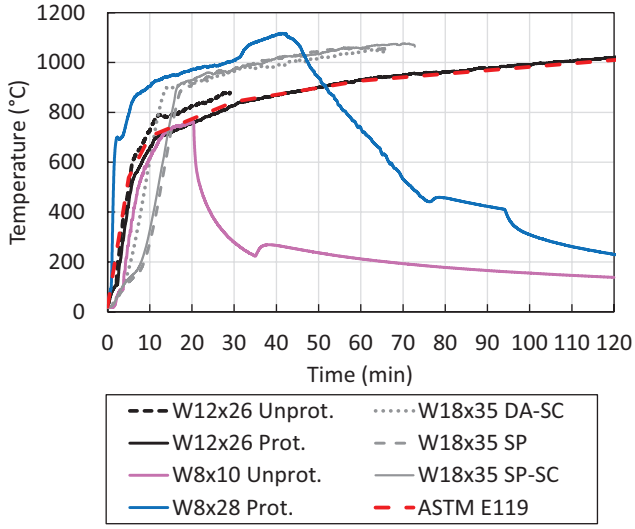

Fig. 3. Temperature-time histories of fire exposures for the tests listed in Table 2.

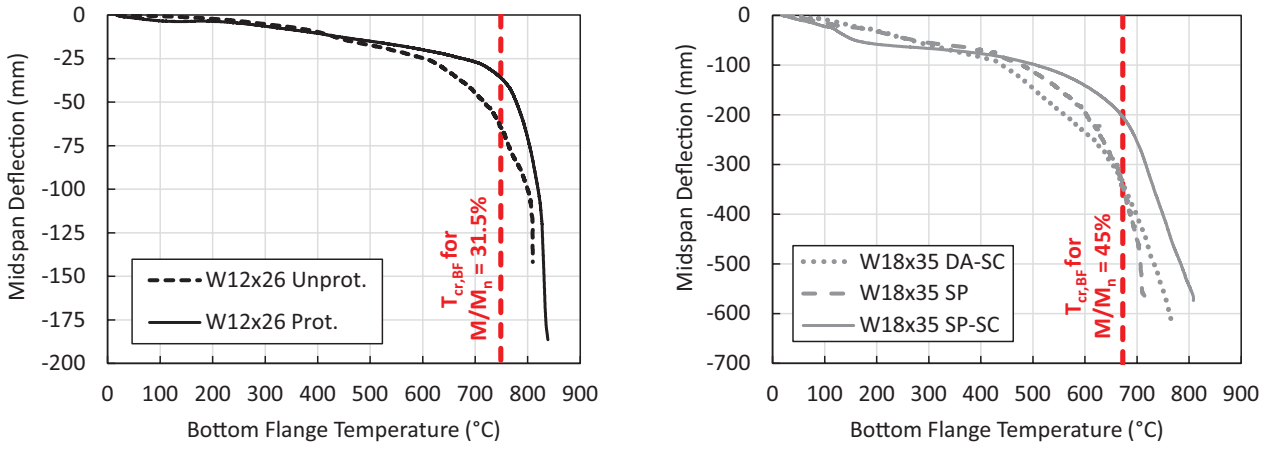

(a) Kordosky et al. (2020) *(b) Choe et al. (2019)*

Fig. 4. Midspan deflection versus $T_{s,BF}$ *from quasi-standard fire tests listed in Table 2 (conversion note: 25 mm = 0.984 in.).*

as the steel temperature increased during the heating phase. However, Figure 5 shows that the peak value of $T_{s,BF}$ for each specimen stopped short of their corresponding value of $T_{cr,BF}$ per Table 1, after which they began to cool during the fire's decay phase and developed significant residual midspan deflection. These test results indicate that $T_{cr,BF}$ as a function of M/M_n per Table 1 can represent a threshold below which a one-way composite beam would be able to maintain its flexural resistance through burnout. The bolted shear tab connections for both specimens exhibited some minor warping damage during post-test inspections but maintained their overall structural integrity (Drury et al., 2021; Drury and Quiel, 2023a). The slabs exhibited some minor post-test cracking but otherwise appeared to be structurally sound and continued to contribute to the residual flexural stiffness of the cooled specimen.

PARAMETRIC MODELING APPROACH

To demonstrate that the relationship for $T_{cr,BF}$ as a function of M/M_n per Table 1 is widely applicable, a modeling approach using fiber-beam elements is used to parametrically analyze the response of three generic composite floor beam assemblies to the fire curves plotted previously in Figure 2. Previous research has shown good agreement between experimental results and this thermo-structural modeling approach for standard [see Chapter 6 of the dissertation by Drury (2022)], quasi-standard (Drury et al., 2020; Drury and Quiel, 2023b), and natural (Drury et al., 2021; Drury and Quiel, 2023b) fire tests of restrained, unrestrained, and partially restrained one-way composite W-shape steel floor beam assemblies. Numerical analysis is conducted via two uncoupled steps: (1) thermal analysis of the fire-exposed structural element cross sections to obtain their temperature increase over the duration of fire exposure (with the fire's temperature-time history used as direct input) and (2) structural analysis of the heated structural assembly (in which the thermal analysis results are used as direct input).

Section and Span Properties

Table 3 summarizes three one-way composite W-shape floor beam configurations that are representative of North American construction practice for steel-frame office buildings (ASCE, 2020; Choe et al., 2019; Sadek et al., 2008). Specifically, the three composite sections were chosen to represent a range of realistic span lengths: 7.3 m (24 ft) for the W14×22, 9.1 m (30 ft) for the W16×26, and 12.2 m (40 ft) for the W18×35. All composite beams [ASTM A992 (2022a) steel with 345 MPa (50 ksi) yield strength] support a 82.6 mm (3.25 in.) lightweight concrete (LWC) slab [with density of 1762 kg/m^3 (110 pcf)] on 76.2 mm (3 in.) corrugated deck (oriented perpendicular to the beam's one-way span) with a compressive strength of 20.7 MPa (3000 psi). The 82.6 mm minimum thickness of LWC generally meets a 2 hr fire resistance rating for thermal transmission thru the slab per ASTM E119 (2024). The slab is reinforced at the mid-depth of its 82.6 mm structural thickness with W1.4×W1.4, 6×6 WWR with 450 MPa (65 ksi) yield strength per ASTM 1064 (2022b). The effective width of the composite slab for its section analysis is taken as $2(L/8)$ per AISC 360-22, Section I3.1a. The beam-slab interface has a single longitudinal line of 19 mm (0.75 in.) shear studs spaced at 304.8 mm (1 ft) above the beam centerline along the entire length of the top flange. This configuration develops 67% composite action based on the relative contributions of the beam, slab, and shear studs to flexural resistance (Vinnakota et al., 1988). It should be noted

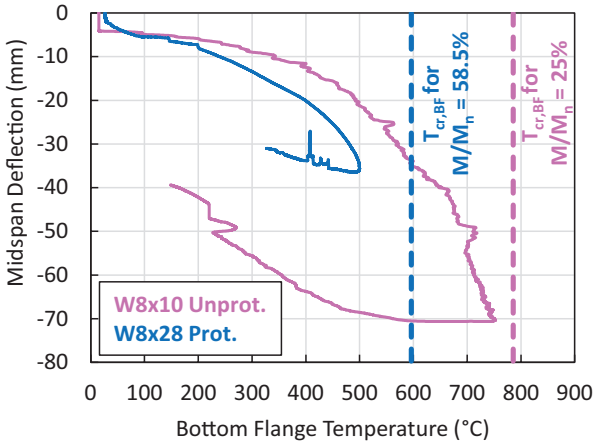

Fig. 5. Midspan deflection versus $T_{s,BF}$ *from natural fire tests listed in Table 2: unprotected W8×10 (Drury et al., 2021) and protected W8×28 (Drury and Quiel, 2023a) (conversion note: 10 mm = 0.394 in.).*

Table 2. Summary of Highlighted Fire Tests from 2019 to 2023 on One-Way Composite Steel Beam Assemblies							
Reference	**Span Length**	**Specimen Description**	**Beam End Conditions**	**Slab End Conditions**	**Protection**	**Fire Exposure**	M/M_n
Kordosky et al. (2020) (2 tests)	10.9 ft	*Beam:* W12×26 *Slab:* 3.25 in. thick on 2 in. profiled deck, 4 ft-8 in. width *Composite action:* 24%	Partial axial restraint with shear tab connection	Unrestrained	Unprotected beam (1 test); 2 hr rated SFRM on the beam (1 test); ceramic fiber blankets for all connections	ASTM E119	31.5%
Choe et al. (2019) (3 tests)	40.0 ft	*Beam:* W18×35 *Slab:* 3.25 in. thick on 3 in. profiled deck, 6 ft width *Composite action:* 82%	Axial restraint with shear tab (SP: 2 tests) or double angle (DA: 1 test) connection	Unrestrained (1 test); axial and rotational restraint to simulate slab continuity (SC: 2 tests)	2 hr rated SFRM on the beam; 3 hr rated SFRM on the connections	Parametric fire that emulated and exceeded ASTM E119	45%
Drury et al. (2021) (1 test)	11.0 ft	*Beam:* W8×10 *Slab:* 2 in. thick on 1.5 in. profiled deck, 4 ft-8 in. width *Composite action:* 52%	Partial axial restraint with shear tab connection	Unrestrained	Unprotected beam; ceramic fiber blankets for all connections	Natural fire with steep decay phase after furnace shutdown	25%
Drury and Quiel (2023a) (1 test)	10.4 ft	*Beam:* W8×28 *Slab:* 2.5 in. thick on 2 in. profiled deck, 4 ft-8 in. width *Composite action:* 97%	Partial axial restraint with shear tab connection	Rotational restraint	2 hr rated SFRM on the beam; ceramic fiber blankets for all connections	Natural fire with controlled decay phase	58.5%

that enhancements to the slab (in particular, an increase in reinforcement quantity or continuity) can enable a modest increase in fire resistance (ASCE, 2020; Gernay and Khorasani, 2020; Khorasani et al., 2019; McAllister, 2014); however, those parameters are outside the scope of this study.

When the underside of the assembly is exposed to fire, the temperature of the steel beam will increase faster than that of the slab, even if the beam is coated with SFRM (Drury et al., 2023a; Kordosky et al., 2020). The temperature of the shear studs will also increase due to conduction from the beam's top flange into the concrete slab; however, testing has shown that the stud temperature is only 75–80% of the top flange temperature (CEN, 2008a; Huang et al., 1999). Also, previous studies have also shown that the presence of slab edge continuity (representative of an actual building system) (Huang et al., 1999) as well as the use of profiled slabs on metal decking (such as that used in this study, rather than a flat slab) (Lim et al., 2020; Mirza and Uy, 2009) will enhance the robustness of the shear studs when the assembly is under fire.

The tensile strength of the steel beam is therefore reduced faster than the compressive strength of the slab or the shear strength of the studs. In recognition of this phenomenon, previous research has shown that composite floor assemblies with ambient composite percentages as low as 24% can rapidly transition to emulating fully composite behavior under fire, even before the fire develops its full intensity (Drury et al., 2020, 2021; Drury and Quiel, 2023a, 2023b; Jiang et al., 2014; Kodur et al., 2013; Kordosky et al., 2020; Wang et al., 2017a, 2017b; Wellman et al., 2011). Analyzing the beam-to-slab interface as fully composite for the purposes of capturing fire-exposed flexural response of the composite member is therefore justified and has been used for parametric numerical analysis on similar composite beam floor systems under fire (Gernay and Khorasani, 2020; Khorasani et al., 2019; Selden and Varma, 2016b, 2016c).

In this study, the composite beam assembly is modeled in SAFIR 2019.a6 (Franssen and Gernay, 2017, 2019) as shown in Figure 6, with separate fiber-beam elements used to represent the steel beam and the structural thickness of the concrete floor slab. Those fiber-beam elements are discretized 304.8 mm (1 ft) lengths based on previously published convergence studies (Drury and Quiel, 2023b;

Quiel and Garlock, 2010). The nodeline for each fiber-beam cross-section runs through its geometric centroid (see Figure 7). A rigid connector link element is used to develop full composite action between the beam and slab at each of their respective nodes.

The one-way span length L is analyzed as uniformly heated, which is commonly assumed for elements in a building compartment with post-flashover fire conditions (which are fully developed and well mixed, thus applying a single temperature-time history of heat exposure to all elements in the compartment). The temperature increases of the W-shape beam section and the composite slab when exposed to fire are calculated separately via uncoupled thermal analyses. The results of those analyses (which are described in the following subsections) are then mapped to the fibers in the cross sections shown in Figure 7.

Based on a previously published convergence study (Drury, 2022), each flange can be represented with a single fiber, and the web can be modeled with 30 equally spaced fibers over its height in order to capture the flexurally induced gradient of strain over the depth of the beam. Temperature-dependent structural properties for the hot-rolled steel beam are taken from Eurocode 3, Part 1-2 (CEN, 2005). The material model assigned to the bottom flange fiber permits the compression-induced onset of local buckling as a reduction of effective yield strength, which represents the reduction of the bottom flange effective width as per the provisions in Eurocode for buckling of unstiffened plates (Franssen et al., 2014). All of the aforementioned long-span fire tests conducted at the National Institute of Standards and Technology (NIST) (Choe et al., 2020) developed local buckling in the bottom flange at the partially restrained ends of the beam but remained stable with reduced end stiffness. Capturing bottom flange local buckling effects is essential for modeling restrained composite beams under fire, particularly for realistic span lengths. Temperature-dependent thermal properties for the steel are also taken from Eurocode 3, Part 1-2 (CEN, 2005) and are conservatively assumed to be reversible during cooling, based on the experimental validation conducted by Drury and Quiel (2023b) for composite floor beams under natural fire exposure.

The LWC slab was modeled with six concrete fibers over its structural thickness, with the WWR represented as a very thin layer at mid-thickness with equivalent area per unit width. Temperature-dependent structural properties for the slab were taken for calcareous concrete per Eurocode 2, Part 1-2 (CEN, 2008b) and include the consideration of explicit transient creep (Gernay and Franssen, 2012). Temperature-dependent structural properties for the WWR were taken for cold-drawn wire per Eurocode 2, Part 1-2 (CEN, 2008b) as well. The slab is assumed to have an in-situ moisture content of 3% and is modeled as having nonreversible thermal properties per Drury and Quiel (2023b), which closely resemble those for LWC in Part 1-2 of Eurocodes 2 and 4 (CEN, 2008a, 2008b).

Flexural Loads

The resulting nominal moment capacity, M_n, for each composite section in accordance with AISC 360-22, Section I3 is summarized in Table 3. Each floor beam is designed as simply supported in one-way bending to support a uniformly distributed line load w, which is assumed to remain constant throughout exposure to fire. For this study, each beam is analyzed for values of w that induce a maximum bending moment at midspan equal to three different percentages of $8M_n/L^2$ as shown in Table 4. These percentages are based on ϕM_n design targets of 30%, 45%, and 60%, with $\phi = 0.90$ per AISC 360-22, Section I3.2a.

In the model, self-weight is applied to each element as a uniformly distributed line load, and superimposed floor loading is applied as a uniformly distributed line load to the slab elements. To induce the initial flexural utilizations listed in Table 4, the value of w in Figure 6 represents the total contributions of self-weight and superimposed floor loads.

End Conditions

These parametric analyses focus on composite W-shape floor beams that are supported with bolted shear connections; girders with moment connections are therefore considered to be outside the scope of this study. These elements are conventionally designed as simply supported under ambient conditions; however, the ends of a heated composite W-shape floor beams in an actual building fire will experience partial (yet significant) restraint against thermally induced expansion and rotation (Moss et al., 2004). That restraint can be provided by the presence of slab continuity beyond the ends of the beam, the beam's connections to surrounding structural elements, as well as the relative stiffness of those supporting elements (Martinez and Jeffers, 2021; McAllister, 2014). Previous research has shown that even a shear connection will realistically exhibit at least some degree of rotational stiffness for floor beams at both ambient conditions (Kishi et al., 1997; Liu and Astaneh-Asl, 2004) and under fire exposure (Choe et al., 2019, 2020; Drury et al., 2021; Drury and Quiel, 2023a; Fischer et al., 2021; Fischer and Varma, 2017; Hantouche et al., 2020; Kordosky et al., 2020). Also, a modest increment of rotational stiffness at the beam ends can have a non-negligible impact on the anticipated structural behavior of the composite beam assembly under fire (Drury and Quiel, 2023b).

For this study, Figure 6 shows that nodal restraint at each end of the beam is approximated via an axial spring with

stiffness K_a and a rotational spring with stiffness K_r. As shown in Table 4, two levels of stiffness are considered for each spring as parameters in this study. The axial restraint low level (aL) is taken equal to $0.1EA_b/L$ for each beam per Dwaikat and Kodur (2011) as a lower-bound estimation of the stiffness provided by the surrounding structure against thermal expansion (where E is the elastic modulus of steel, A_b is the cross-sectional area of the beam, and L is the span length). The axial restraint high level (aH) is taken as a constant value of 190 kN/mm (1085 kip/in.), which was used by the aforementioned study on fire-exposed one-way composite beams at NIST (Choe et al., 2019, 2020; Ramesh et al., 2019) to represent a typical lateral restraining stiffness in a steel framed building. To represent a realistic upper bound of stiffness for a shear connection, the rotational stiffness high level (rH) for K_r is taken as $2EI_b/L$, which is the limiting value per AISC 360-22, Section C-B3.4, below which a connection can be considered simple (where I_b is taken as the steel beam's moment of inertia). The rotational stiffness low level (rL) is arbitrarily taken as 1/20th of that limiting value at $0.1EI_b/L$.

It should be noted that these stiffnesses are kept constant throughout each simulation, even though the connections and slab end conditions would realistically experience temperature-induced weakening and potential permanent deformation by restraining the beam's expansion and rotation (Block et al., 2013; Burgess et al., 2012; Garlock and Selamet, 2010; Hantouche et al., 2020). However, previous research has demonstrated that applying constant beam-end stiffness (similar to the models for this study) can enable close numerical predictions of flexural tests results for partially restrained one-way composite W-shape steel floor beam assemblies under quasi-standard (Drury et al., 2020; Drury and Quiel, 2023b), and natural (Drury et al., 2021; Drury and Quiel, 2023b) fire exposure. An explicit evaluation of the connections is beyond the scope of this study; however, the impact of natural fire exposure on connection reactions will be addressed later in this paper.

As shown in Figure 6, two additional slab elements are included beyond each end of the beam as an approximate representation of slab continuity. For simplification, the horizontal translation at the end node of this slab extension is constrained to that at the end of the beam (which is attached to the axial spring with stiffness, K_a). The vertical translation and rotation of the two slab nodes beyond the end of the beam are restrained, thus implying that the slab extension is compositely attached to the framing that supports the beam. When the assembly experiences a significant increase in fire-induced deflection, the slab extension elements will undergo tensile cracking via its strain compatibility with the rotating end of the composite beam. At this point, the WWR layer in the slab extension will become realistically engaged in a tensile hogging response.

Passive Fire Protection

Each floor beam is analyzed for three levels of passive fire protection (see Table 4): unprotected (i.e., bare steel) and two thicknesses of contour coated lightweight SFRM [with a density of 240 kg/m^3 (15 pcf), emulating the commonly used commercial product CAFCO 300 (Isolatek

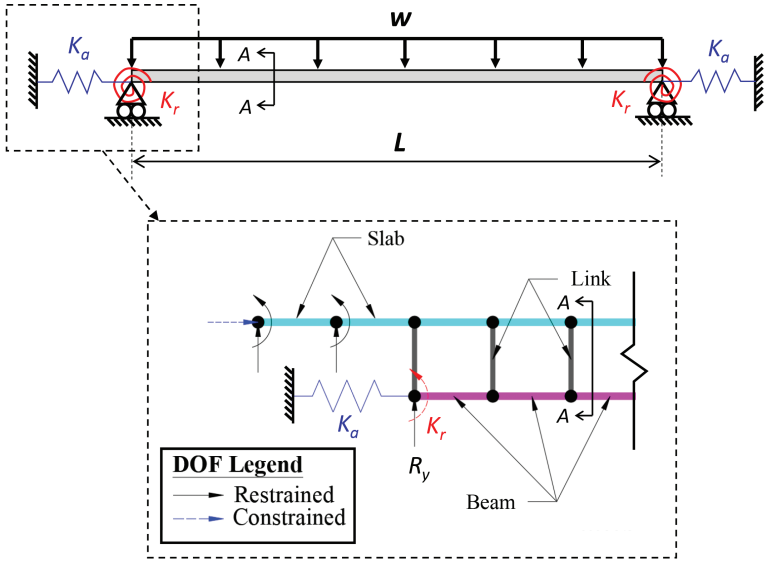

Fig. 6. Elevation schematic of the FE model used for parametric study of the one-way composite floor beam configurations in Tables 3 and 4.

Table 3. Summary of Generic Composite Floor Beam Configurations for Parametric Analysis						
Reference	Span Length (ft)	Beam Section	Slab Section	Composite Section M_n (kip-ft)	P1 SFRM Thickness (in.)	P2 SFRM Thickness (in.)
Sadek et al. (2008)	24	W14×22	3.25 in. LWC on 3 in. deck	277	7/16	7/8
ASCE (2020)	30	W16×26		361	7/16	7/8
Choe et al. (2019)	40	W18×35		535	3/8	13/16

Table 4. Matrix of Modeling Parameters				
Beam Section	Passive Fire Protection Level	Flexural Utilization (M/M_n)	Beam End Axial Stiffness (K_a)	Beam End Rotational Stiffness (K_r)
W14×22 W16×26 W18×35	Unprotected (U) 1 hr protected (P1) 2 hr protected (P2)	27.0% 41.5% 54.0%	aL: $0.1EA_b/L$ aH: 1085 k/in.	rL: $0.1EI_b/L$ rH: $2EI_b/L$

International, 2020)]. Composite floor members in Type I building construction are required to meet a 2 hr fire resistance rating per IBC Table 601 (ICC, 2023). This requirement is commonly met by selecting a 2-hr-rated SFRM thickness from UL Designs in the D900, N700, and N800 series (UL, 2022a), which are determined via ASTM E119 standard fire testing results for a particular composite section configuration. The published thickness for the tested beam in the selected UL design would then be adapted to the actual beam using the conversion equations in AISC 360-22, Section A-4.3.2c, which are a function of the relative section factors (i.e., the ratio of cross-sectional area divided by fire-exposed perimeter) between the two beams.

In this study, two thicknesses of lightweight SFRM are selected per UL D902 (UL, 2022b): P1 corresponds to a 1 hr unrestrained beam rating, and P2 corresponds to a 2 hr assembly rating (restrained and unrestrained). The resulting fire protection thicknesses, summarized in Table 3, are tailored to each W-shape section via the aforementioned conversion equations and rounded up to the nearest 1.58 mm (1/16 in.) increment, in accordance with typical practice. Note that the 1 hr unrestrained beam rating per UL D902 can also be used to represent a 2 hr restrained/unrestrained assembly rating per UL D982 (UL, 2022c), based on comparative fire testing completed in 2013 by AISC and AISI (Alfawakhiri et al., 2016; Carter and Alfawakhiri, 2013).

Temperature-dependent thermal properties for the SFRM are taken as the mean value of the stochastic functions proposed by Khorasani et al. (2015) (specifically, Equations 22 to 24 and Figure 9 from that paper). Those equations align well with the results of experimental testing for CAFCO 300 [see Chapter 7 of the dissertation by Drury (2022)] and other commercially available SFRMs of similar "lightweight" density (Carino et al., 2005; Harmathy, 1965; Jeanes, 1984; Kodur and Shakya, 2013). The temperature-dependent thermal properties for the SFRM are also conservatively assumed to be reversible during cooling, based on the experimental validation conducted by

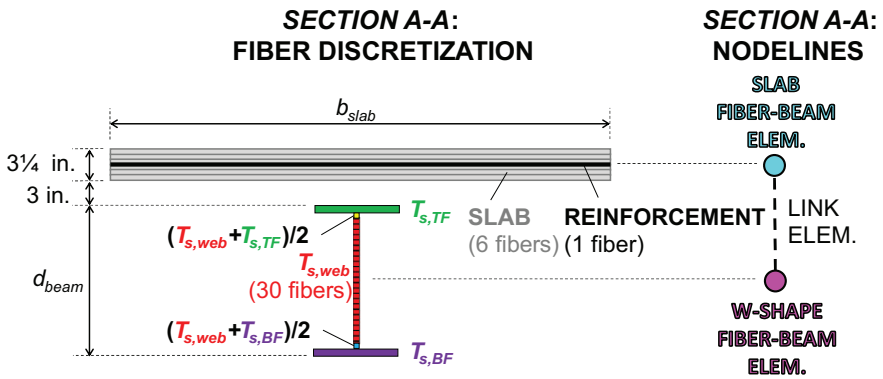

Fig. 7. Details of section A-A from Figure 6.

Drury and Quiel (2023b) for composite floor beams under natural fire exposure.

Fire Exposures

Standard fire temperature-time histories, such as those specified in ASTM E119 (2024) (see Figure 2), UL 263 (2020), or ISO 834 (2019), undergo a rapid rise past 800°C (1472°F) in the first 30 min, followed by a more gradual increase to ~1100°C (~2012°F) after 2 hr. The fire temperature then increases indefinitely with no subsequent decay phase until the assembly reaches a specified thermal or structural limit. Again, the application of standard fire curves constitutes the basis for hourly ratings per SFRD.

ASCE recently commissioned a series of PBSFD examples for generic steel framed buildings that were performed by several leading structural design firms in partnership with academic experts in structural fire engineering (ASCE, 2020). The temperature-time histories of the three natural fire curves in Figure 2 are reproduced from Chapter 7 of that report for a 1,277 m^2 (13,746 ft^2) compartment floor area with either high or low ventilation. The baseline fuel load of 374 MJ/m^2 (32.9 $kBtu/ft^2$) represents the 80% fractile fuel load per Eurocode 1, Part 1-2 (CEN, 2009), including a risk reduction factor for automatic sprinklers. An elevated fuel load of 912 MJ/m^2 (80.3 $kBtu/ft^2$) neglects the risk reduction factor for sprinklers and represents the 98% fractile fuel load (Khorasani et al., 2014). As shown in Figure 2, the curves FH374 (natural fire with high ventilation and 374 MJ/m^2 fuel load), FL374, and FH912 represent a range of intensities that exceed that of the ASTM E119 standard fire curve within the first ~20 min of the fire but then burn out with varying decay rates due to their differences in ventilation.

Parametric Model Configurations

The parametric matrix in Table 4 produces 108 total model configurations, which are named according to their parameters. For example, model name W14-U-27-rHaL denotes a W14×22 beam section with no SFRM (unprotected), initially loaded to 27% flexural utilization (M/M_n), with high rotational stiffness and low axial stiffness at the ends of the beam. Each model configuration is then subjected to each of the four temperature-time histories for fire exposure in Figure 2: the ASTM E119 standard fire, and natural fires FH374, FL374, and FH912.

THERMAL ANALYSIS: STEEL BEAM CROSS SECTION

The flanges and web are each represented as a lumped mass that absorbs heat from the fire and conducts heat between adjacent plates and to the composite slab. An experimentally validated three lumped mass (3LM) analysis, presented in Section 4.1 of the paper by Drury et al. (2020), is used to calculate the temperatures in each steel plate over the duration of fire exposure; for brevity, those equations are not recounted here. All surfaces of the bottom flange and web are assumed to be uniformly exposed to the fire's temperature-time history. The bottom and side surfaces of the top flange are also uniformly exposed to fire; its top surface, however, is in partial contact with the floor slab. Due to the corrugated deck, it is assumed that half of the top surface of the top flange is in contact with the slab. Conductive heat transfer from the top flange to the slab through that contact area is calculated using the closed-form relationship proposed by Ghojel and Wong (2005). For unprotected beams, the half of the top surface of the top flange that is not in contact with the slab is conservatively included in its fire-exposed perimeter (Drury et al., 2020, 2021). For protected beams, the gap between the top flange and the deck flutes is assumed to be filled with SFRM, which is common practice for this type of floor system (Drury and Quiel, 2023a; Kordosky et al., 2020). The half of the top surface of the top flange that is not in contact with the slab is considered to be heavily insulated by the SFRM infill and is therefore neglected when calculating the fire-exposed perimeter.

The fire-exposed perimeter of the SFRM for the protected beams is assumed to have the same temperature as the fire at any given time step, and heat transfer to the steel is calculated via conduction across the SFRM thickness. This assumption is common practice for fire-exposed surfaces of SFRM-protected steel sections (AISC, 2022; CEN, 2005). Heat transfer to the fire-exposed surfaces of unprotected beams is calculated using the following thermal boundary conditions:

- The convective heat transfer coefficient is taken as 25 W/m^2-K (4.4 $Btu/hr\text{-}ft^2\text{-}°F$) for surfaces heated by all fire exposures and 4 W/m^2-K (0.7 $Btu/hr\text{-}ft^2\text{-}°F$) for unheated surfaces or during cooling for natural fire exposure. It should be noted that Eurocode 3, Part 1-2 (CEN, 2005) recommends a convective coefficient of 35 W/m^2-K (6.2 $Btu/hr\text{-}ft^2\text{-}°F$) for surfaces heated by natural fire exposure; for this study, however, the same convective coefficient was used for all fire curves to maintain consistency in the thermal boundary conditions for direct comparison.

- Eurocode 3, Part 1-2 (CEN, 2005) recommends a resultant emissivity of 0.7 but with the potential inclusion of a shadow effect factor, which is dependent on the width of the bottom flange relative to the depth of the web. However, a reduced resultant emissivity of 0.5 is used as an implicit application of shadow effects for all sections based on previous experimental validations by Drury et al. (2020, 2021).

Preliminary 3LM thermal calculations indicated that a time step of 30 s was acceptably small to achieve a convergent thermal solution (Drury et al., 2020, 2021; Gamble, 1989).

The resulting time histories of $T_{s,BF}$, $T_{s,TF}$, and T_{web} from 3LM heat transfer analysis of the beam sections in Table 3 are plotted in Figure 8 for exposure to the ASTM E119 standard fire as well as the FH374 natural fire. The curves for $T_{s,BF}$ and T_{web} track closely together in all cases regardless of the presence or amount of passive fire protection. Also, the three beam section sizes exhibit similar thermal responses on a plate-by-plate basis for each passive fire protection case. The temperatures in all three plates of the unprotected beams are not only very similar, but closely follow the fire curve during heating. As the SFRM thickness is increased, the plates heat progressively slower, as would be expected. During the decay phase of the natural fire, the bottom flange and web cool at a faster rate than the top flange because they have a greater section factor (i.e., the ratio of exposed perimeter to cross-sectional steel area).

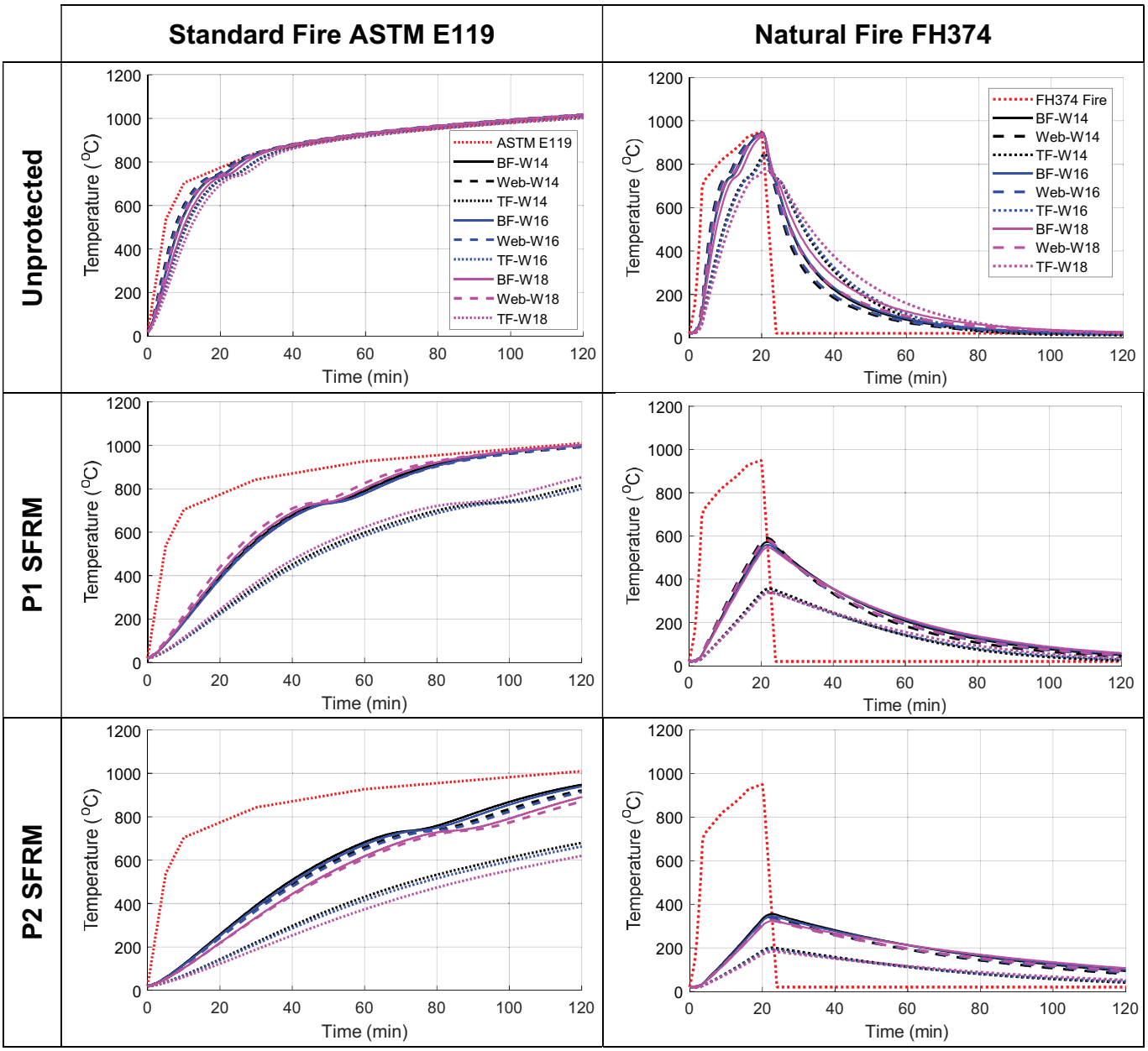

Fig. 8. Calculated temperature-time histories for the flange and web plates of the generic composite beam configurations under standard and natural fire exposure.

The steel temperatures for each lumped mass are then mapped to the 32 fibers in the beam cross section shown previously in Figure 7 as thermal input for structural FE analysis in SAFIR. $T_{s,BF}$ and $T_{s,TF}$ are assigned to their respective single fibers, and $T_{s,web}$ is assigned to the innermost 28 fibers in the web. The fibers at the top and bottom of the web are each used as transition elements and are taken as the average of the lumped mass temperatures from the web and adjacent flange plate. Preliminary modeling explored the application of a linear thermal gradient between mid-height of the web and the top flange [as suggested in AISC 360-22, Section A-4.2.4d(f)]; however, structural FE results were relatively unaffected, and the simpler approach outlined above was therefore used for all parametric analyses in this study.

THERMAL ANALYSIS: CONCRETE SLAB CROSS SECTION

Concrete has significantly less thermal diffusivity and thermal mass compared to steel, and the slab will therefore develop a thermal gradient through its thickness. For this reason, lumped mass methods are not appropriate for thermal analysis of the slab, which is instead examined via one-dimensional heat transfer analysis in SAFIR 2019.a6 (Franssen and Gernay, 2017, 2019). To account for the non-uniform thickness of the slab on the corrugated metal deck, two analyses are initially conducted for each fire exposure: the 82.8 mm (3.25 in.) "thin" section of the slab is vertically divided into 6 equal fibers, and the 158.8 mm (6.25- in.) "thick" section is likewise divided into 11 equal fibers as shown in Figure 9. The structural thickness of

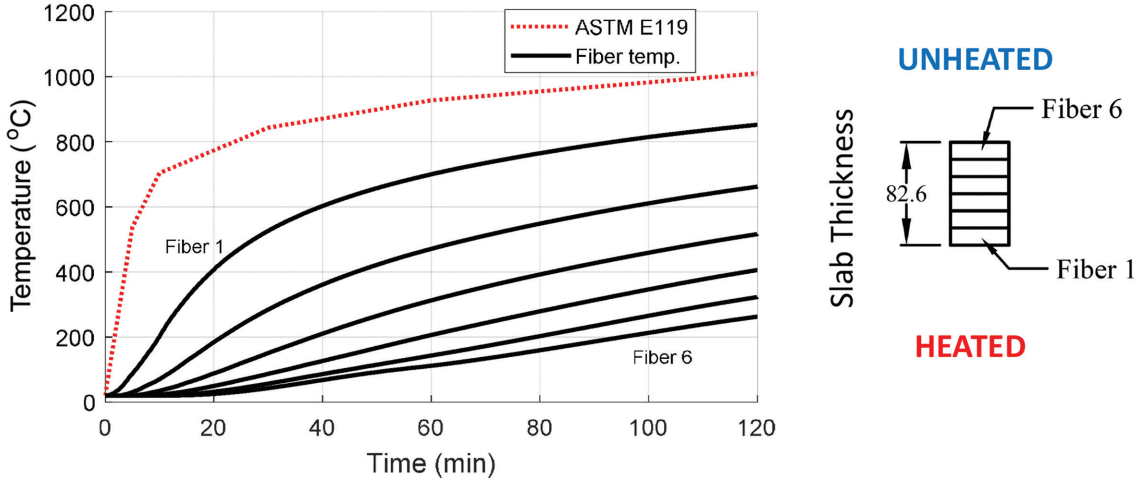

(a) 82.6 mm (3.25 in.) thin slab

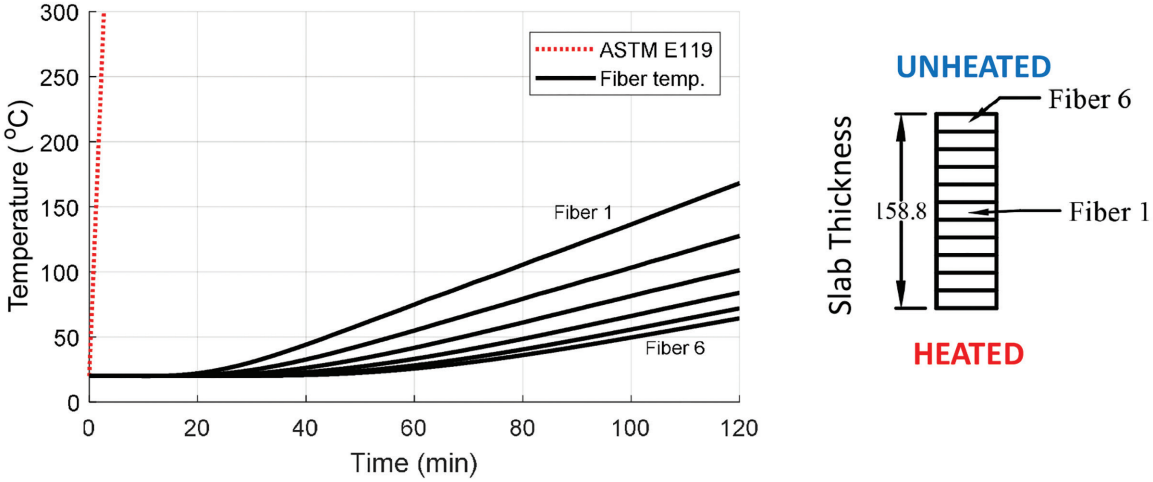

(b) 158.8 mm (6.25 in.) thick slab

Fig. 9. Fiber temperature-time histories for the thin and thick models of the concrete slab.

the slab is 82.8 mm (3.25 in.) thick and is taken as having the same 6-fiber discretization as the "thin" section. The temperature-time history in each fiber of the structural thickness under each fire exposure is calculated as a weighted average per Drury and Quiel (2023b) among all 6 fibers from the thin section and the upper 6 fibers from the thick section.

Convective heat transfer coefficients are taken as 25 W/m^2-K (4.4 Btu/hhr-ft^2-°F) for heated surfaces and 4 W/m^2-K (0.7 Btu/hr-ft^2-°F) for surfaces that are either not exposed to fire (such as the top surface of the slab) or cooling during the decay phase of a natural fire (CEN, 2008b; Drury and Quiel, 2023b). The resultant emissivity of the bottom surface of the slab is taken as 0.3 to account for shadow effect and reflectivity of the galvanized corrugated metal deck (Kodur et al., 2013). Note that the WWR at the mid-depth of the structural thickness is not explicitly included in the one-dimensional thermal models of the slab. Due to its low thermal mass and high conductivity relative to the LWC, the WWR would have a negligible impact on the thermal response of the LWC. Rather, the temperature of the WWR is simply taken as the average of neighboring fibers when using these thermal results as input for structural modeling.

The fiber temperature-time histories of the thick and thin slab sections are plotted in Figure 9 for exposure to the ASTM E119 standard fire. The resulting weighted average fiber temperatures for the slab's structural thickness are then shown in Figure 10. Fiber temperatures under natural fire exposure show a similar gradient through the slab thickness and are therefore not plotted here for brevity. Based on previously published research (Drury et al., 2020; Gernay and Khorasani, 2020; Wang, 2012), the fully composite assumption (and, in turn, the lack of consideration of stud temperatures) is justified since the temperature of the steel beam (in particular the bottom flange, which is critical in providing tensile resistance in flexure) will always outpace the temperature of not only the slab, but also the concrete-encased shear studs due to the inherent geometry of composite floor construction. Because full composite action is assumed in the structural model, the heating of shear studs is also not addressed. This simplification is further justified based on the experimental validation study previous conducted by Drury and Quiel (2023b) for similar composite beam specimens under standard and natural fire exposure.

FLEXURAL RESPONSE TO STANDARD FIRE EXPOSURE

The calculated midspan deflections for all composite beam configurations under ASTM E119 standard fire exposure are plotted in Figures 11, 12, and 13 (W14×22, W16×26, and W18×35, respectively) for all three levels of SFRM protection and for all levels of end restraint per Table 4. For brevity, each plot shows only the 27% and 54% flexural utilization levels because the results of these cases effectively bracket the results of the 40.5% utilization cases. Also included on each plot are several horizontal lines that correspond to the following deflection limits, which have conventionally been used to describe the loss of flexural resistance in one-way beam spans under fire:

- A deflection limit equal to $L/20$ or $L/30$ has been used as a practical stopping point for numerous standard fire tests on one-way composite steel floor beams (Jiang et al., 2017; Wang et al., 2017a; Choe et al., 2020). This level

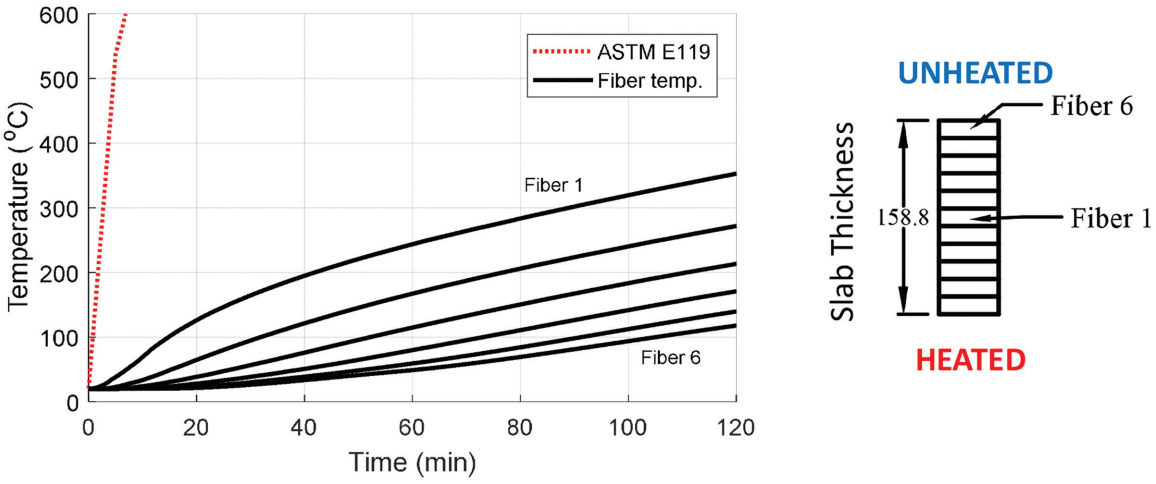

Fig. 10. Fiber temperature-time histories for the 82.6 mm (3.25 in.) structural thickness of the concrete slab, calculated as a weighted average of like fibers from the thick and thin section analyses.

of deflection is sufficiently large to imply the engagement of tensile membrane action in the beam (Martinez and Jeffers, 2021). The larger of these two limits, $L/20$, is marked on the plots of midspan deflection in Figures 11, 12, and 13.

- A deflection limit equal to $L^2/(400d)$ (where d is the distance between extreme fibers in the flexural cross-section) is used in combination with a limiting deflection rate for standard fire tests per ASTM E119 (ASTM, 2024) to approximate the loss of flexural resistance for loaded unrestrained beams. This deflection limit has been used in previous studies to also evaluate restrained beams, with d taken as either the steel beam depth, d_{beam}, (Rackauskaite et al., 2019; Selden, 2014) or the total depth of the steel beam plus the composite slab thickness, d_{comp} (Alfawakhiri et al., 2016; Kordosky et al., 2020). The values of $L^2/(400d_{beam})$ and $L^2/(400d_{comp})$ are both marked on Figures 11–13 for comparison.

All models exhibit a similar trend of midspan deflection when exposed to the ASTM E119 standard fire, regardless of the level of fire protection or beam end restraint. As the beam initially heats up, the deflection gradually increases until the onset of nonlinear stress-strain behavior in the heated beam, at which point the deflection rate increases.

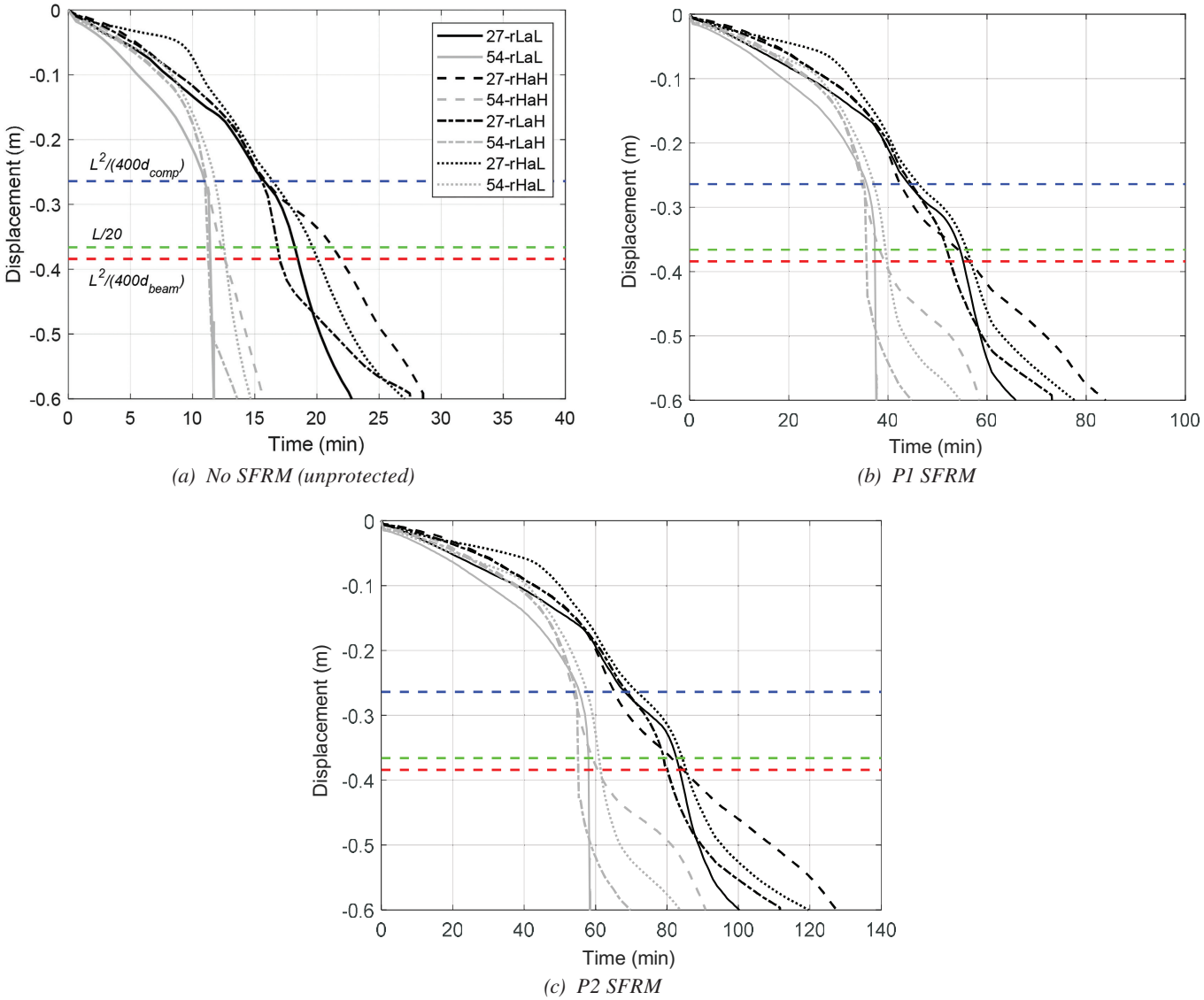

(a) No SFRM (unprotected)

(b) P1 SFRM

(c) P2 SFRM

Fig. 11. Midspan deflection for the one-way W14×22 composite beam configuration under ASTM E119 standard fire exposure with varying levels of SFRM per Table 4 (conversion note: 0.1 m = 3.94 in.).

Nonlinear behavior is generated by thermally induced losses of strength and stiffness as well as an increase in internal force due to the restraint of thermal expansion. As expected, higher flexural loading and lower rotational restraint on the beam ends (rL) enable an earlier increase in deflection rate. Once the deflection exceeds $L/20$, then the composite beam transitions from flexural response to a catenary response. Most models experience a slight stiffness recovery during the catenary phase due to the composite interaction of the beam and slab before eventually losing all resistance and reaching nonconvergence. A few models such as W14-U-57-rLaL plunge to runaway deflection almost immediately after losing flexural resistance due to the low axial and rotational stiffness at the ends of the composite beam.

The values of $T_{s,BF}$ at which each model reaches the three deflection milestones are plotted in Figure 14(a–c) as a function of initial flexural utilization. Figure 14(d) plots the $T_{s,BF}$ at the onset of an axial tension reaction at the ends of the beam, thus indicating a transition to catenary behavior. This milestone is structurally significant: If the connections and continuous slab can resist these tensile reactions, then the beam can develop additional fire resistance in the catenary state. If the connections fail under these reactions,

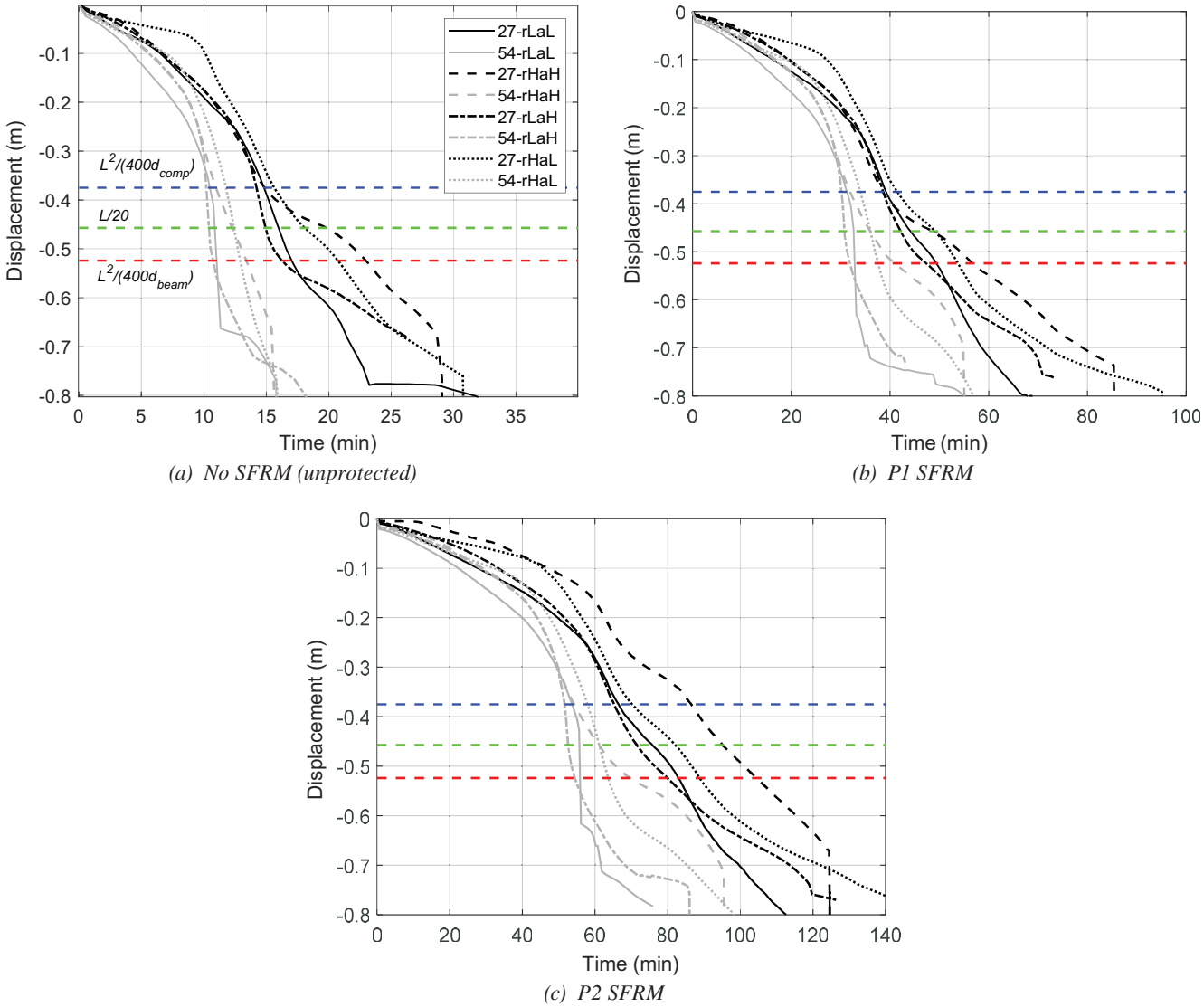

(a) No SFRM (unprotected)

(b) P1 SFRM

(c) P2 SFRM

Fig. 12. Midspan deflection for the one-way W16×26 composite beam configuration under ASTM E119 standard fire exposure with varying levels of SFRM per Table 4 (conversion note: 0.1 m = 3.94 in.).

then the assembly may collapse. The values of $T_{s,BF}$ in Figure 14(d) would therefore represent the true loss of flexural resistance; any subsequent catenary response can be regarded as a redundancy or hardening prior to ultimate failure.

It should be noted that standard fire tests per ASTM E119 (ASTM, 2024) and ISO 834 (ISO, 2019) are typically performed on specimens with bearing-plate end supports, rather than a realistic connection to the test fixture. If tested as restrained, the bearing ends of the beam will develop axial compression and rotational restraint in response to thermal expansion. However, a transition from flexural response to catenary action is not possible for those test specimens because the beam end can simply pull away from the horizontal bearing support (which cannot offer any axial tensile resistance) when flexural resistance is lost. The beam will therefore approach a runaway deflection rate soon after the loss of flexural resistance. The reader is referred to the previous paper by Drury and Quiel (2025) for more illustration of the end conditions for composite beam specimens in standard fire tests.

The values of $T_{s,BF}$ in Figures 14(a) and 14(b) for the $L/20$ and $L^2/(400d_{comp})$ deflection milestones are much lower (i.e., more conservative) compared to those in Figure 14(d) for the onset of catenary response. Those in Figure 14(c) for $L^2/(400d_{beam})$, however, show good overall agreement with

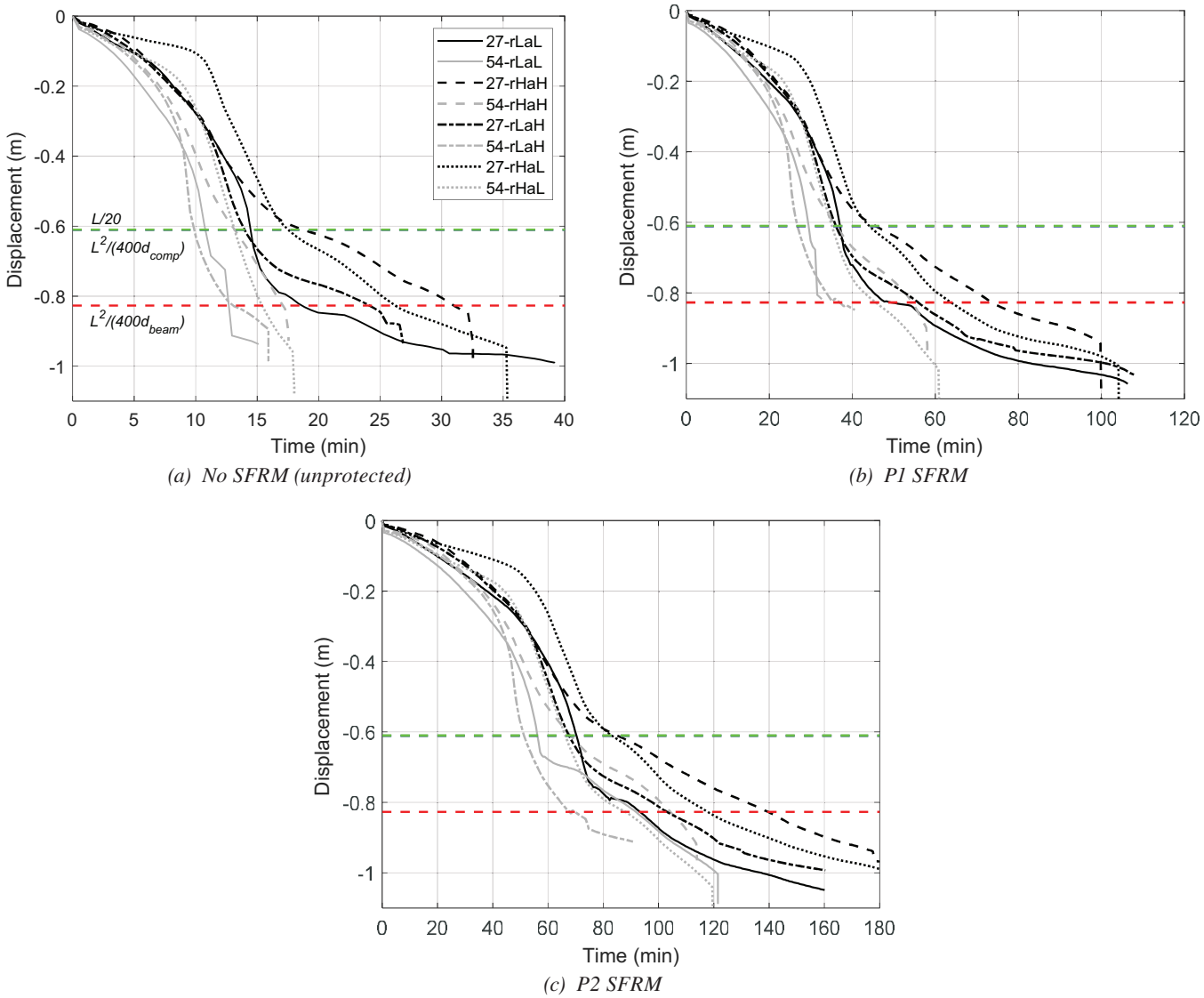

(a) No SFRM (unprotected)

(b) P1 SFRM

(c) P2 SFRM

Fig. 13. Midspan deflection for the one-way W18×35 composite beam configuration under ASTM E119 standard fire exposure with varying levels of SFRM per Table 4 (conversion note: 0.2 m = 7.87 in.).

those in Figure 14(d), though with a slightly greater vertical dispersion at each load level. These results indicate that the $L^2/(400d_{beam})$ can be used to appropriately denote the loss of flexural resistance under fire, which is consistent with previous work by Rackauskaite et al. (2019).

For comparison, the plots in Figure 14 also include two representations of critical bottom flange temperature, $T_{cr,BF}$: one per AISC 360-22, Table A-4.2.4 (reproduced previously in Table 1), and the other a constant value of $T_{cr,max} = 704°C$ (1300°F) per ASTM E119. The plotted $T_{s,BF}$ for all models in Figures 14(c) and 14(d) either fall above or very close to the load-dependent curve for $T_{cr,BF}$. This outcome is consistent with a recent review of standard fire tests on a wide range of one-way composite floor beam configurations (Drury and Quiel, 2025) and reinforces the notion that the moment retention factor per AISC 360-22, Table A-4.2.4, can serve as an appropriate load-dependent relationship for $T_{cr,BF}$ at the loss of flexural resistance under standard fire exposure. The constant $T_{cr,max}$ per ASTM E119, on the other hand, fails to capture the influence of initial flexural loading on the fire-induced response of these one-way composite beams.

In Figures 15 through 18, the midspan deflection for each model is normalized by its corresponding value of $L^2/(400d_{beam})$ and plotted against $T_{s,BF}$ for all four parametric combinations of beam end restraint in the following order: rLaL, rHaH, rLaH, and rHaL. The value of $T_{cr,BF}$ per AISC 360-22, Table A-4.2.4, for the corresponding level of applied loading is also marked on these plots as a vertical line—again, plots are provided only for initial flexural utilizations of 27% and 54% for brevity. Once the beams develop significant nonlinear stress-strain behavior at a deflection equaling 30–40% of $L^2/(400d_{beam})$, all models show a noticeable acceleration in deflection rate. These figures consistently show a loss of flexural resistance (following an acceleration of deflection) for all models under standard fire exposure when $T_{s,BF}$ reaches $T_{cr,BF}$ and the midspan deflection approaches $L^2/(400d_{beam})$. This outcome is robust across all parameters, including beam section size, one-way span length, the level of applied fire protection, the level of applied loading, and the level of beam end restraint.

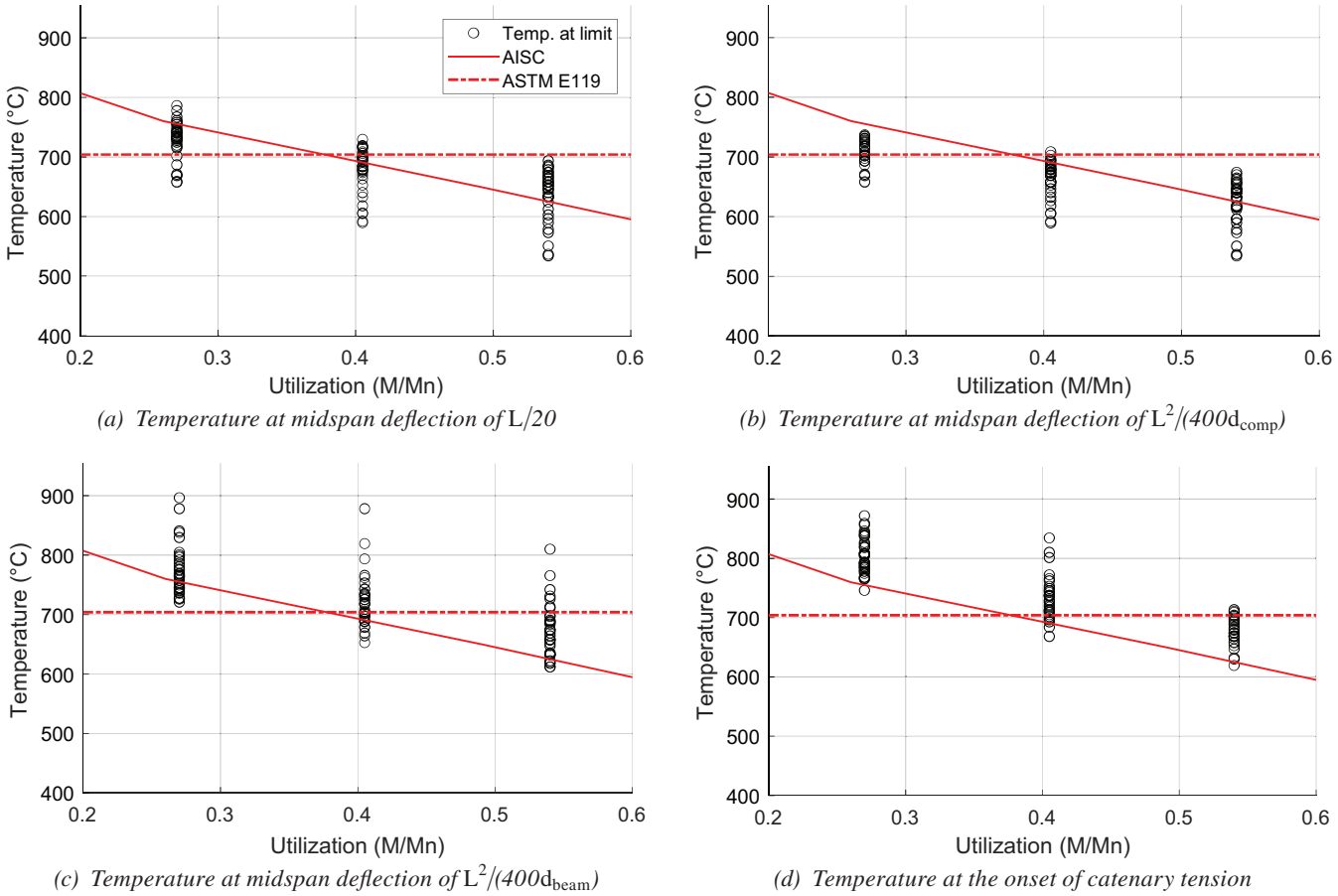

(a) Temperature at midspan deflection of $L/20$

(b) Temperature at midspan deflection of $L^2/(400d_{comp})$

(c) Temperature at midspan deflection of $L^2/(400d_{beam})$

(d) Temperature at the onset of catenary tension

Fig. 14. $T_{s,BF}$ *versus initial flexural utilization at several structural response milestones for all models under ASTM E119 fire exposure.*

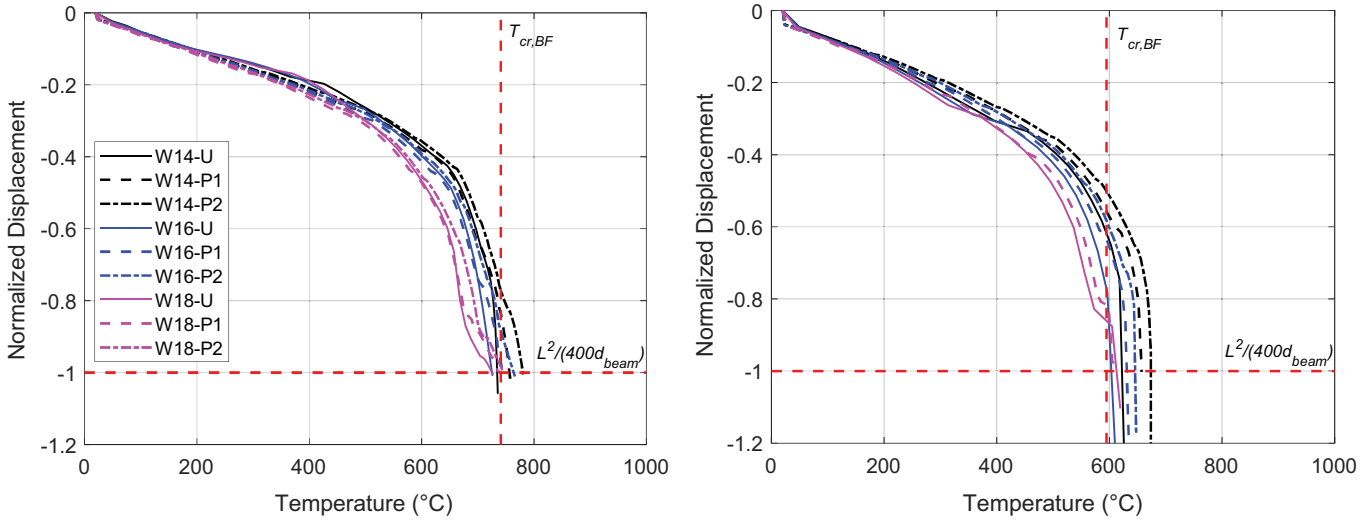

(a) 27% initial flexural utilization *(b) 54% initial flexural utilization*

Fig. 15. Midspan displacement [normalized by the corresponding value of $L^2/(400d_{beam})$] versus $T_{s,BF}$ under ASTM E119 fire exposure with rLaL restraint.

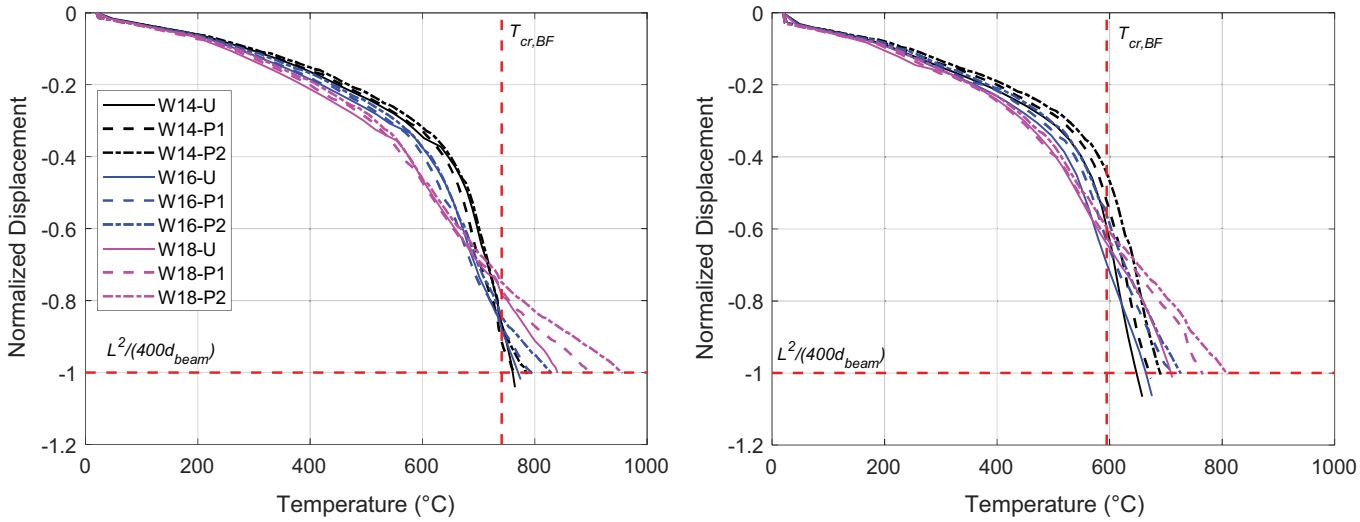

(a) 27% initial flexural utilization *(b) 54% initial flexural utilization*

Fig. 16. Midspan displacement [normalized by the corresponding value of $L^2/(400d_{beam})$] versus $T_{s,BF}$ under ASTM E119 fire exposure with rHaH restraint.

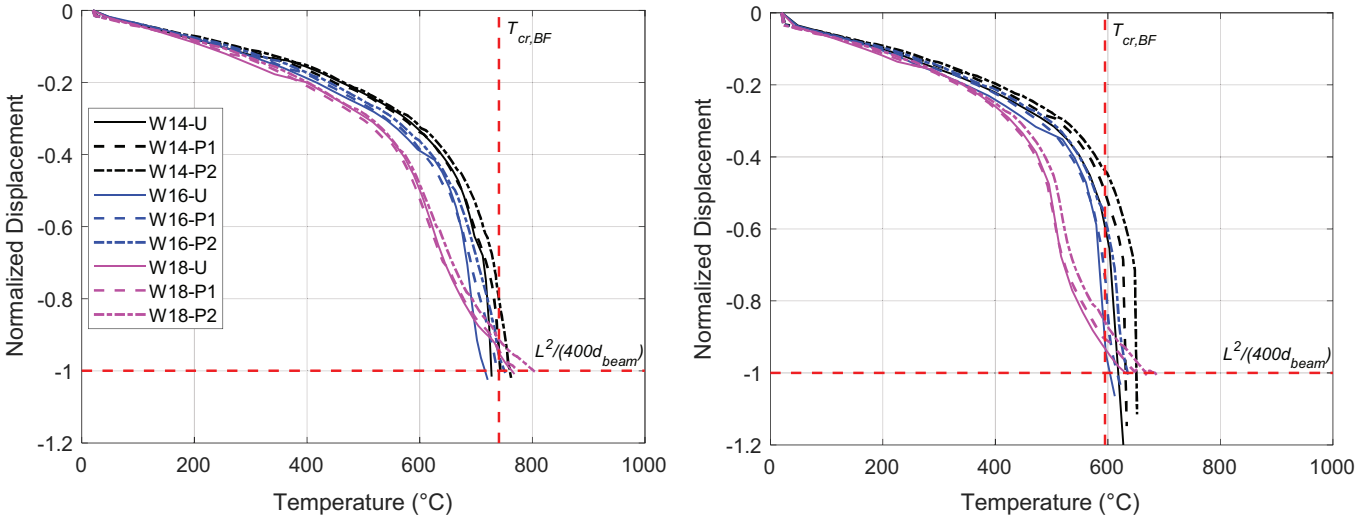

(a) 27% initial flexural utilization *(b) 54% initial flexural utilization*

Fig. 17. Midspan displacement [normalized by the corresponding value of $L^2/(400d_{beam})$] versus $T_{s,BF}$ under ASTM E119 fire exposure with rLaH restraint.

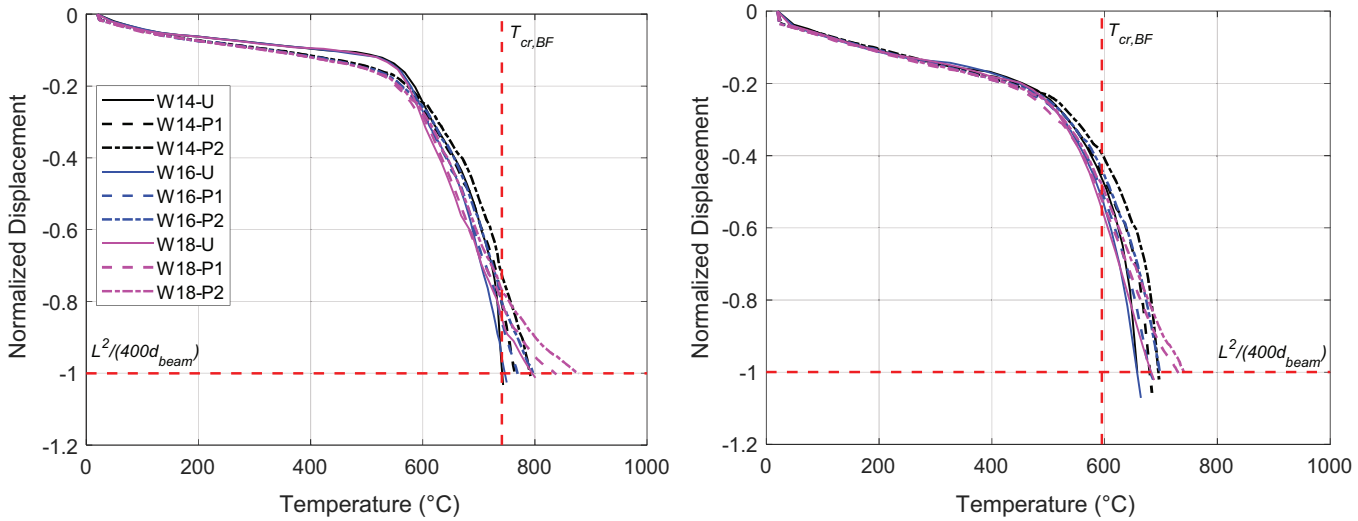

(a) 27% initial flexural utilization *(b) 54% initial flexural utilization*

Fig. 18. Midspan displacement [normalized by the corresponding value of $L^2/(400d_{beam})$] versus $T_{s,BF}$ under ASTM E119 fire exposure with rHaL restraint.

FLEXURAL RESPONSE TO NATURAL FIRE EXPOSURE

The calculated midspan deflections for all 108 composite beam configurations when exposed to the FH374 natural fire curve are plotted in Figures 19, 20, and 21 (W14×22, W16×26, and W18×35, respectively) for all three levels of SFRM protection and for all levels of end restraint per Table 4. As before, each plot shows only the 27% and 54% flexural utilization levels for brevity and includes a horizontal "limit" line corresponding a deflection of $L^2/(400d_{beam})$. Similar to the standard fire results in Figures 11–13, the results in Figures 19(a), 20(a), and 21(a) show that all unprotected beams experience a loss of flexural resistance during the heating phase of the FH374 fire and reach the $L^2/(400d_{beam})$ deflection milestone before proceeding to numerical nonconvergence.

When SFRM is applied, the (b) and (c) plots in Figures 19, 20, and 21 show that all composite beam configurations are able to survive the FH374 fire exposure through burnout. All protected beams experience a rapid increase in deflection during the active heating phase and then partially rebound to a stable magnitude of residual deflection when cooling during the decay phase. As expected, models with

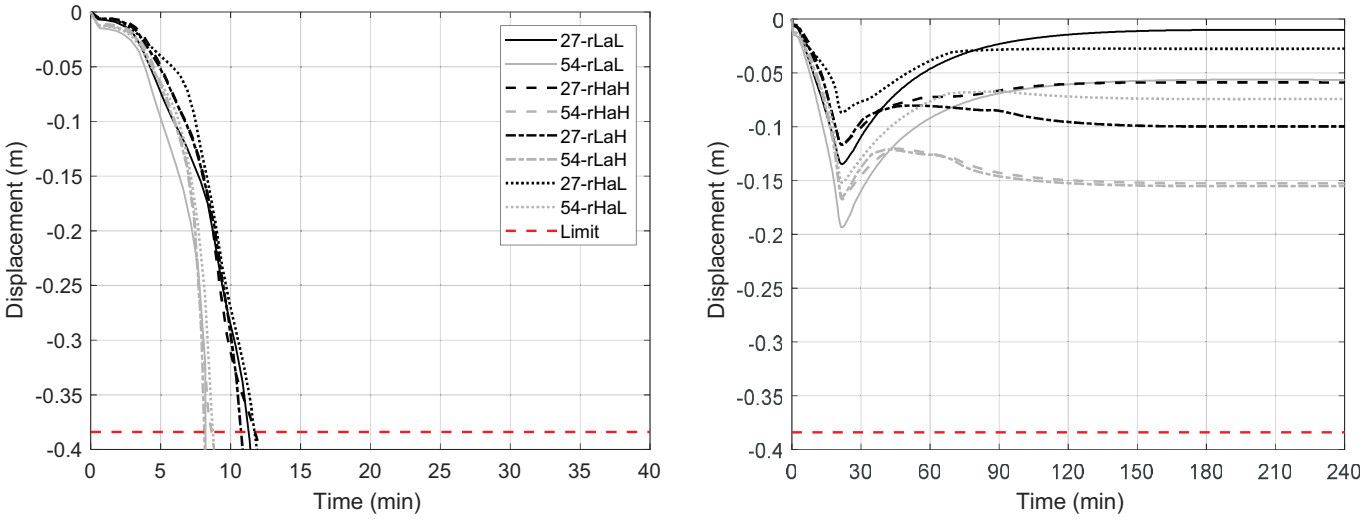

(a) No SFRM (unprotected)

(b) P1 SFRM

(c) P2 SFRM

Fig. 19. Midspan deflection for the one-way W14×22 composite beam configurations under FH374 natural fire exposure with varying levels of SFRM per Table 4 (conversion note: 0.05 m = 1.97 in.).

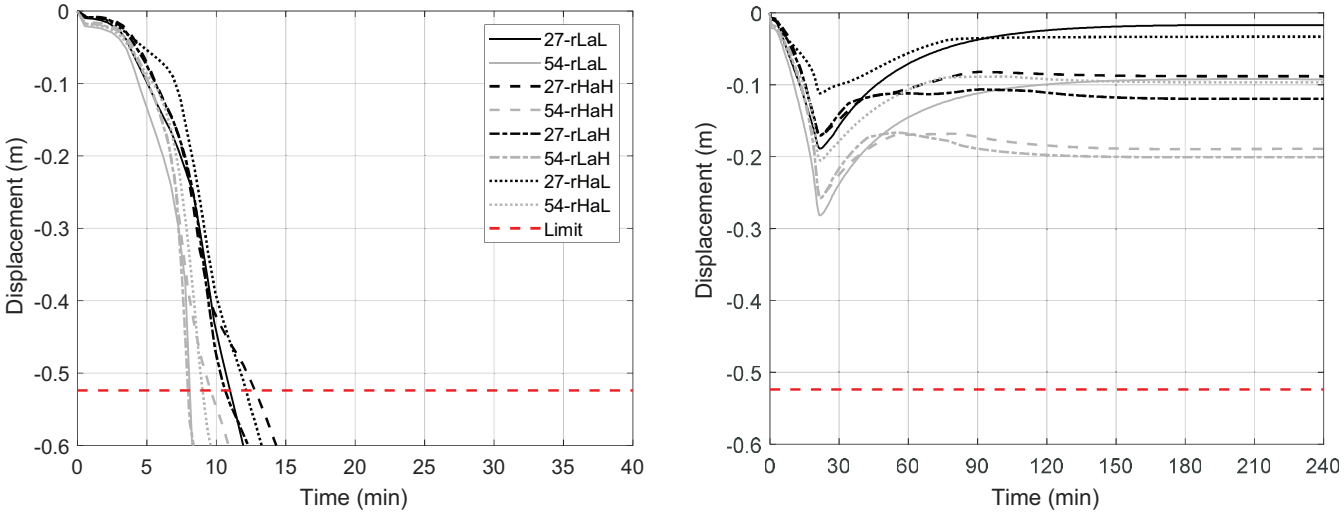

(a) No SFRM (unprotected)

(b) P1 SFRM

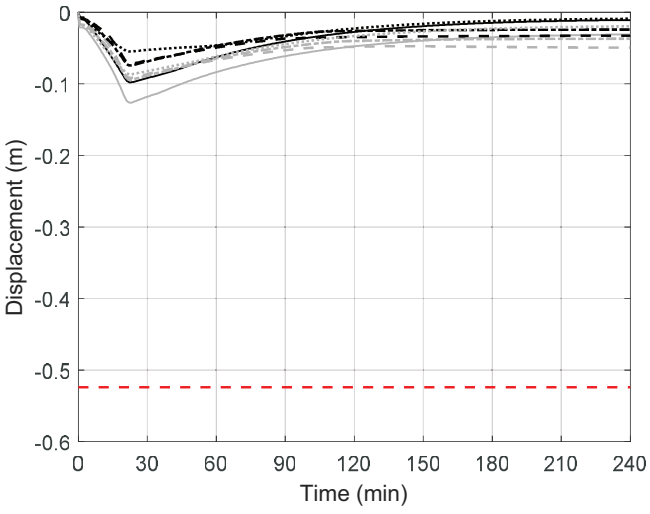

(c) P2 SFRM

Fig. 20. Midspan deflection for the one-way W16×26 composite beam configurations under FH374 natural fire exposure with varying levels of SFRM per Table 4 (conversion note: 0.1 m = 3.94 in.).

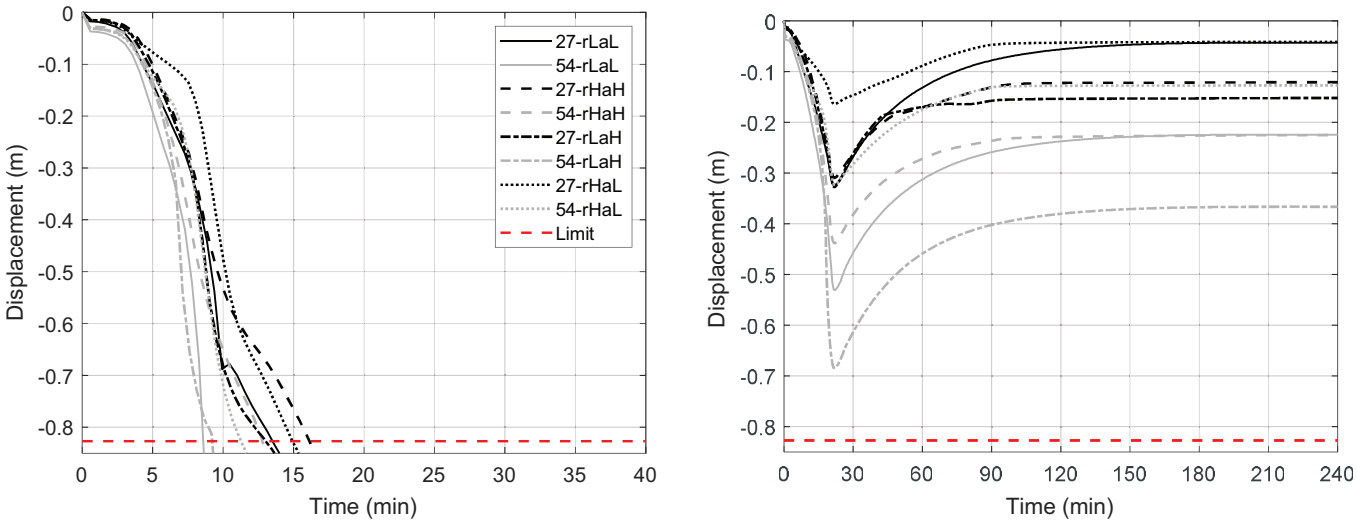

(a) No SFRM (unprotected)

(b) P1 SFRM

(c) P2 SFRM

Fig. 21. Midspan deflection for the one-way W18×35 composite beam configurations under FH374 natural fire exposure with varying levels of SFRM per Table 4 (conversion note: 0.1 m = 3.94 in.).

rL beam end restraint develop the largest peak deflections during heating by providing less direct resistance. Those with aH beam end restraint develop the largest magnitudes of residual deflection during cooling; these beams develop larger internal forces in response to higher axial restraint of thermal expansion, which thereby translates into larger permanent deflection once the assembly has cooled. Overall, models with higher levels of applied loading and the lower level of SFRM develop greater overall magnitudes and rates of deflection.

Calculated midspan deflections are plotted in Figures 22 and 23 for select composite beam configurations when exposed to the FL374 and FH912 natural fire curves, respectively. The responses of unprotected beam configurations to these fire curves are very similar to those shown in Figures 19(a), 20(a), and 21(a) for exposure to the FH374 natural fire and are therefore not plotted for brevity. Also, results are shown only for models with rL beam end restraint because they develop larger deflections and thus a more severe fire-induced response than those with rH beam

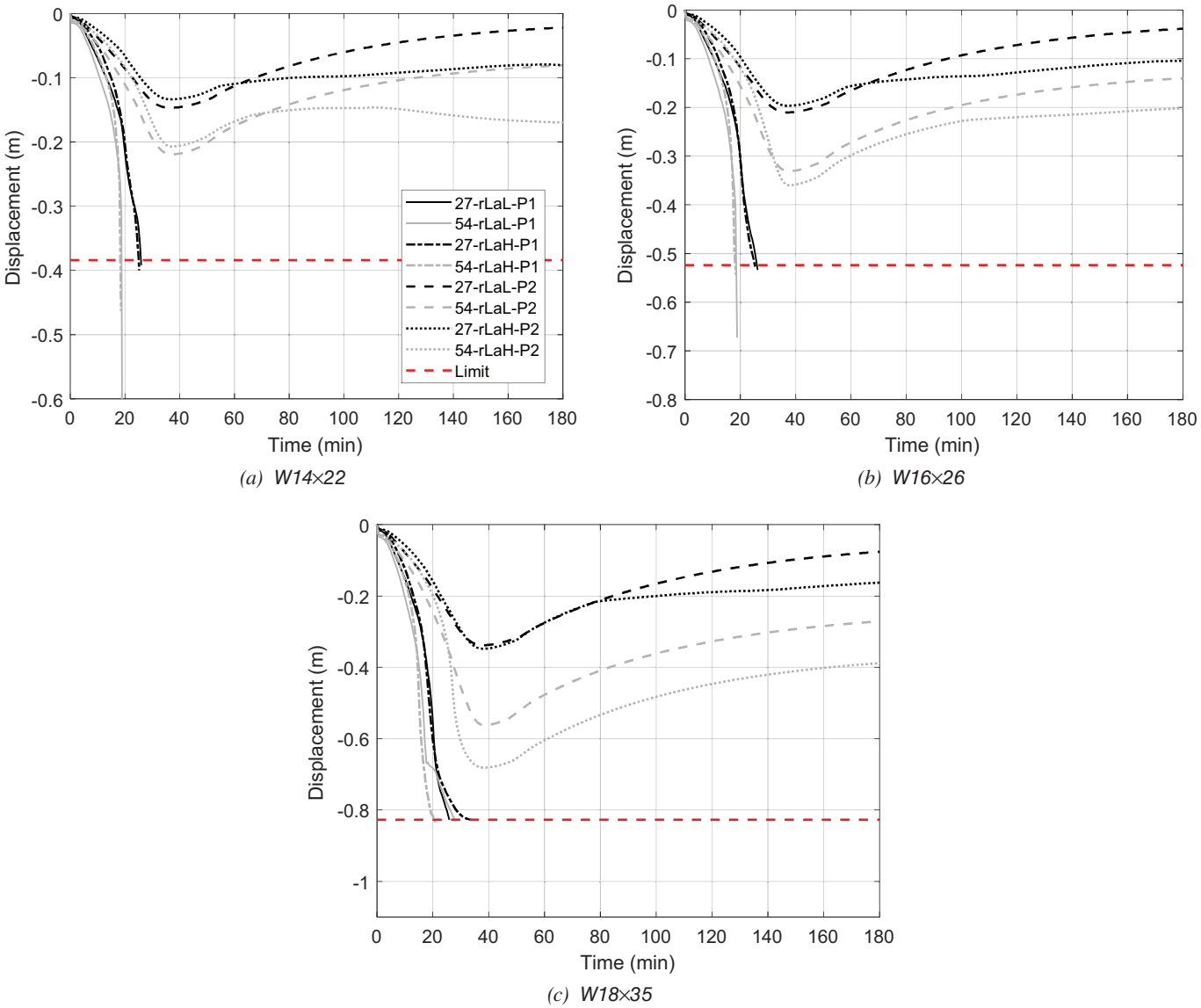

(a) W14×22

(b) W16×26

(c) W18×35

Fig. 22. Midspan deflection under FL374 natural fire exposure for composite beam configurations with rL restraint and P1 and P2 SFRM (conversion note: 0.1 m = 3.94 in.).

end restraint. As shown previously in Figure 2, the FL374 and FH912 fire curves are more severe (in terms of both maximum temperature and total duration) compared to that for FH374; as a result, the deflections for all P1 SFRM protected beam configurations in Figures 22 and 23 now also experience a loss of flexural resistance during the heating phase of these fires and reach the $L^2/(400d_{beam})$ deflection milestone before proceeding to numerical nonconvergence. Beams with the thicker P2 SFRM protection survive these fire exposures through burnout and develop stable residual deflection when cooling. As before, models with larger applied loading develop larger peak deflections, and models with aH beam end restraint develop larger residual deflections. Some of the models [particularly, W18–54-rLaH under the FH912 fire in Figure 23(c)] come very close to the $L^2/(400d_{beam})$ deflection limit before the heating phase ends, after which the beam is still able to develop a stable residual state with significant permanent deflection.

Similar to the standard fire results in Figure 14(c), Figure 24 shows that the values of $T_{s,BF}$ at a midspan deflection of $L^2/(400d_{beam})$ for the unprotected beams exposed to the FH374 natural fire curve are again above or very close to the load-dependent curve for $T_{cr,BF}$ per AISC 360-22, Table A-4.2.4. Similar to Figures 15–18, the midspan

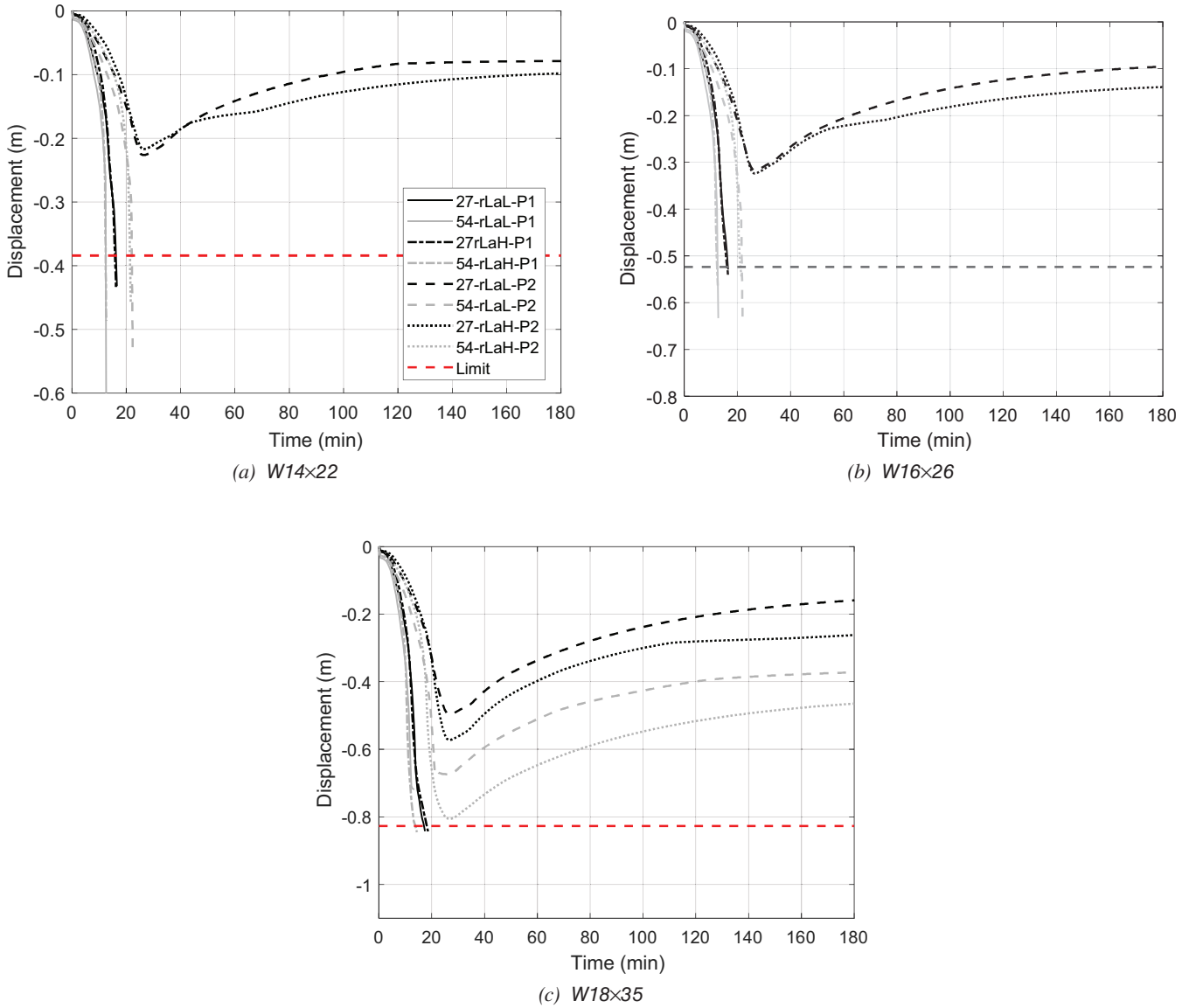

(a) W14×22

(b) W16×26

(c) W18×35

Fig. 23. Midspan deflection under FH912 natural fire exposure for composite beam configurations models with rL restraint and P1 and P2 SFRM (conversion note: 0.1 m = 3.94 in.).

deflection plotted previously for every SFRM-protected beam exposed to FH374 [Figures 19(b–c), 20(b–c), and 21(b–c)], FL374 (Figure 22), and FH912 (Figure 23) is normalized by its corresponding value of $L^2/(400d_{beam})$ and plotted against its $T_{s,BF}$ in Figures 25, 26, and 27. In these plots, all models that suffer a loss of flexural stiffness reached the intersection of the horizontal line for the $L^2/(400d_{beam})$ deflection limit with the vertical line for $T_{cr,BF}$ per AISC 360-22, Table A-4.2.4. Similar to the results for standard fire exposure, all models again show a noticeable acceleration in deflection rate once the deflections reach 30–40% of $L^2/(400d_{beam})$. All models that survive their respective natural fire curve experience a maximum $T_{s,BF}$ during the heating phase that clearly falls short of the vertical line for $T_{cr,BF}$ and partially rebounds to a residual deflection achieved during cooling. The magnitude of residual deflection is influenced by the maximum value of $T_{s,BF}$, the total duration of heating, the level of beam end restraint, and the level of applied loading, as well as the composite beam geometry. A full exploration of the influence of these parameters on residual deflections is outside the scope of this paper but are an important consideration for the selection of passive fire protection that can minimize damage and enable a speedier restoration of post-fire functionality

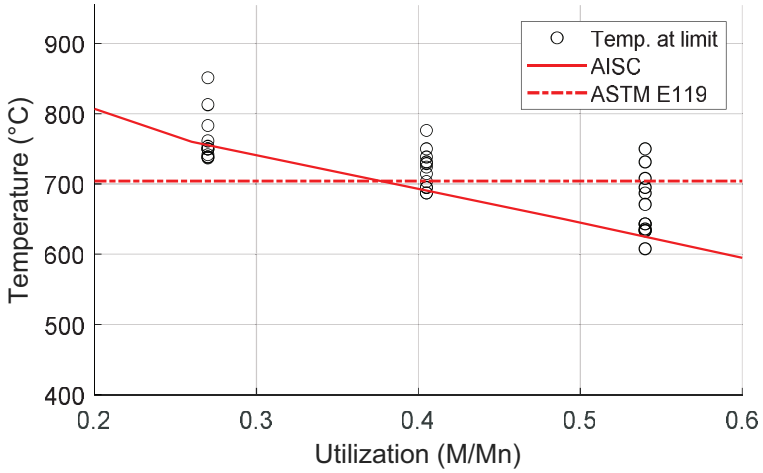

Fig. 24. $T_{s,BF}$ at a midspan deflection of $L^2/(400d_{beam})$ versus initial flexural utilization for all unprotected composite beam configurations under FH374 natural fire exposure.

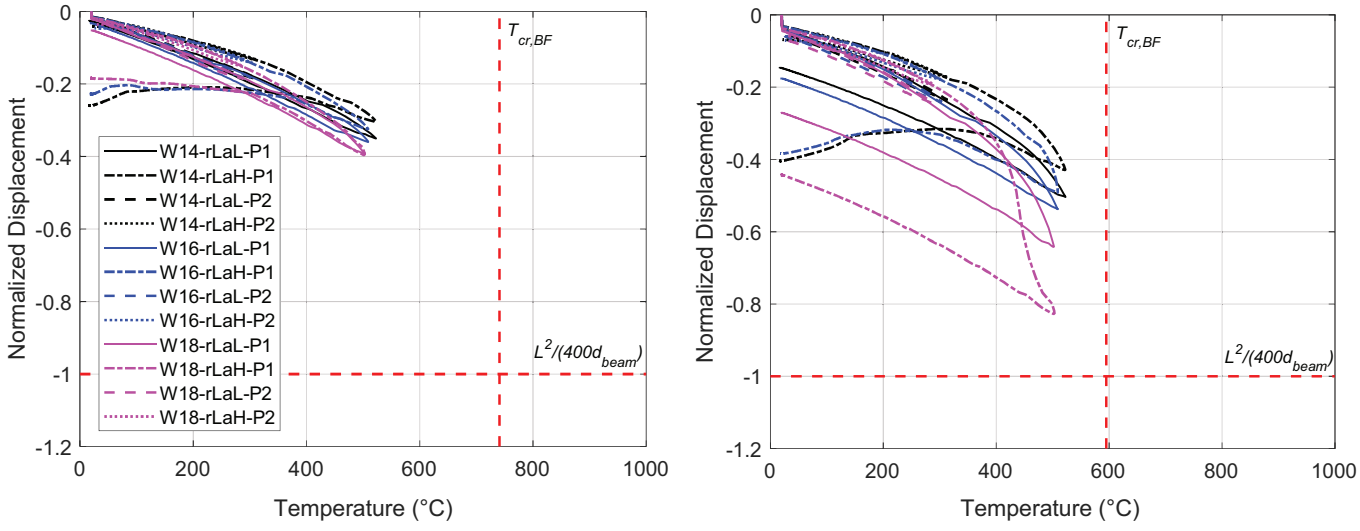

(a) 27% initial flexural utilization

(b) 54% initial flexural utilization

Fig. 25. Midspan displacement [normalized by the corresponding value of $L^2/(400d_{beam})$] versus $T_{s,BF}$ under FH374 natural fire exposure for models with rL restraint and P1 and P2 SFRM.

(i.e., to enhance the resilience of these assemblies against natural fire exposure).

Commentary on Connection Reactions

The axial forces at the beam ends from the models subjected to the FH374 natural fire are plotted in Figures 28, 29, and 30 for the W14×22, W16×26, and W18×35 composite floor beam configurations, respectively. For rLaL models with the lowest level of beam end restraint, the residual tensile forces that develop during cooling are small compared to the compressive forces developed from the restraint of thermal expansion during heating. Specifically, these cases experience less permanent compressive strain due to lower restraint of thermal expansion during heating. Models with higher beam end restraint develop more permanent shortening when heated and therefore develop more residual tension in their connections when cooling. This outcome suggests that an optimal end restraint lies

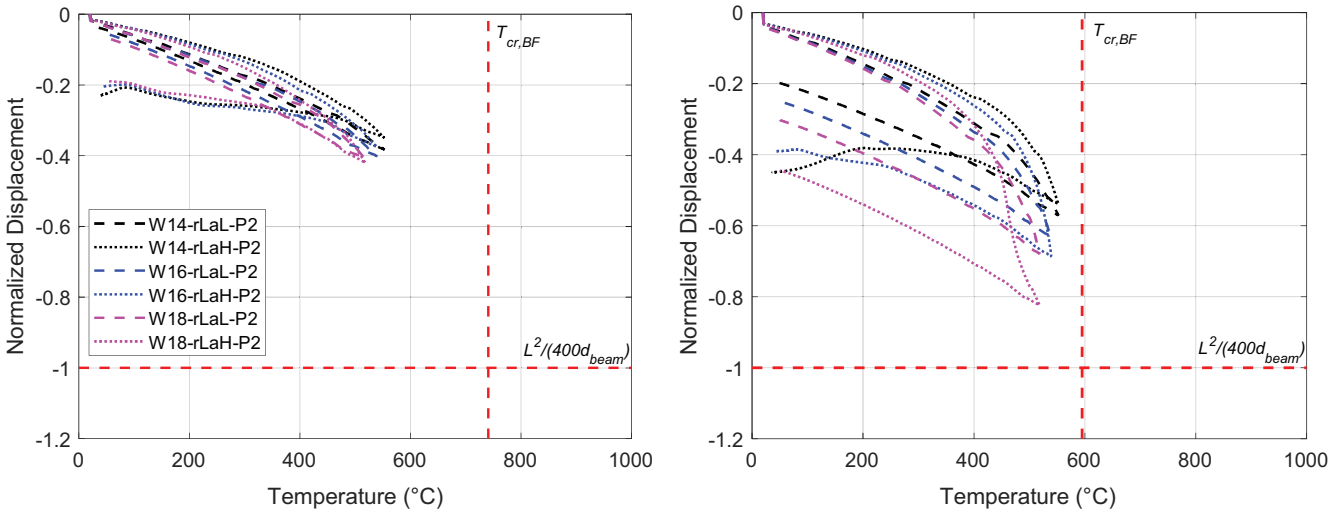

(a) 27% initial flexural utilization *(b) 54% initial flexural utilization*

Fig. 26. Midspan displacement [normalized by the corresponding value of $L^2/(400d_{beam})$*] versus* $T_{s,BF}$ *under FL374 natural fire exposure for models with rL restraint and P2 SFRM.*

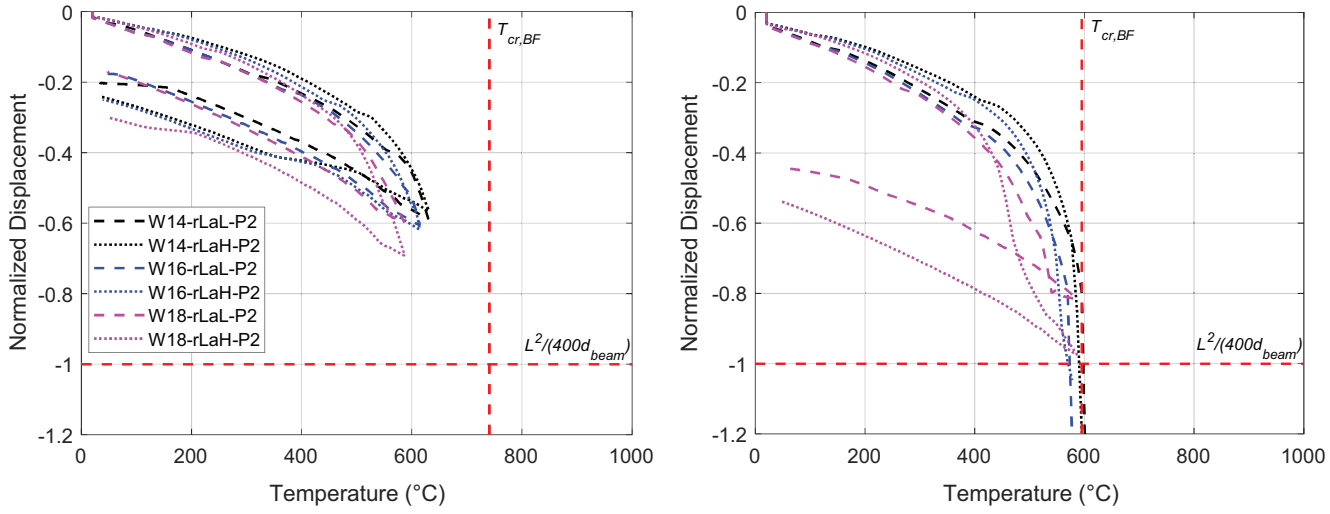

(a) 27% initial flexural utilization *(b) 54% initial flexural utilization*

Fig. 27. Midspan displacement [normalized by the corresponding value of $L^2/(400d_{beam})$*] versus* $T_{s,BF}$ *under FH912 natural fire exposure for models with rL restraint and P2 SFRM.*

somewhere between fully restrained and fully unrestrained (LaMalva et al., 2020; Moss et al., 2004). Conversely, Figures 28–30 show that the aH models develop the largest magnitudes of residual tension at their beam ends. Also, models with the lower P1 SFRM thickness develop higher beam temperature; the translation of the associated thermal expansion into larger restraining stresses therefore produces larger magnitudes of residual tension in these beams than their counterparts with the larger P2 SFRM thickness.

Due to the use of idealized beam end conditions, the values plotted in Figures 28–30 are not exact but instead represent an approximate range of reaction demands that the shear connections would experience due to natural fire exposure. To fully achieve a performance-based, fire-resistant design, the tensile capacity of the shear connections at the beam ends must be capable of withstanding these residual reactions. Large-scale tests on composite floor assemblies have shown that connection failures are possible both during heating as well as significantly after

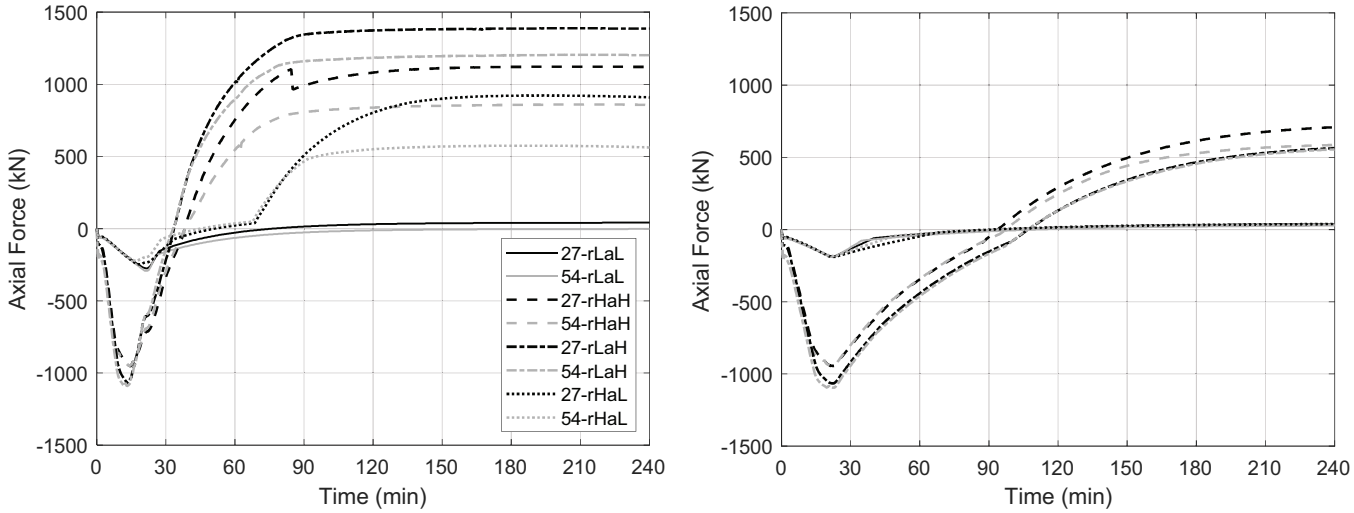

(a) P1 SFRM *(b) P2 SFRM*

Fig. 28. Beam end axial force for the W14×22 composite beam configurations under FH374 natural fire exposure with varying levels of SFRM (conversion note: 500 kN = 112.4 kips).

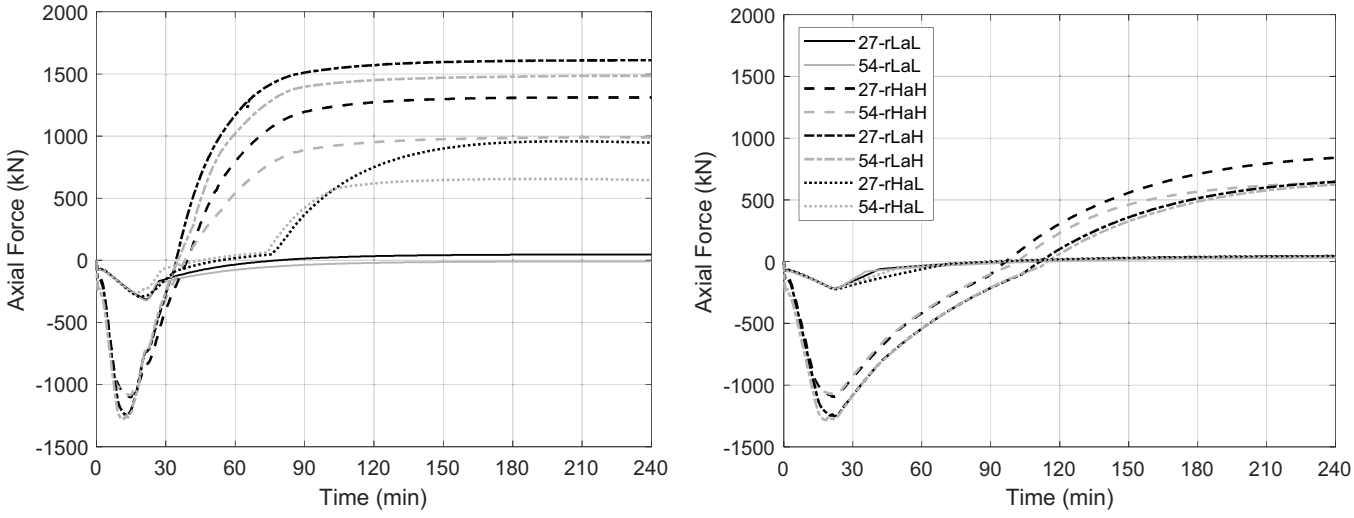

(a) P1 SFRM *(b) P2 SFRM*

Fig. 29. Beam end axial force for the W16×26 composite beam configurations under FH374 natural fire exposure with varying levels of SFRM (conversion note: 500 kN = 112.4 kips).

natural fire burnout while the deformed beam cools and contracts (Choe et al., 2019; Selden et al., 2016a). Rotational and tensile capacities of shear connections under fire have been investigated in several previous studies (Block et al., 2013; Liu and Astaneh-Asl, 2004; Seif et al., 2013; Selamet and Garlock, 2010; Yu and Frank, 2009); however, there is little consensus to date as to how these connections should be designed to survive natural fire exposure.

It should be noted that the simplified structural model used for this study applies the rotational and axial end restraint to the full cross-sectional area of the steel beam; however, shear connections for floor beams typically have a web attachment only. When the composite beam is heated, the bottom flange can come into contact with the supporting framing element via thermal expansion as well as end rotation from large deflection. Localized compression from this contact can induce local buckling in the bottom flange plate, thereby mitigating compression via damage absorption (Kordosky et al., 2020). Connection reactions during heating can also be reduced due to web local buckling or bolt slip within the connection (Hantouche et al., 2020; Liu and Astaneh-Asl, 2004). The top flange additionally transmits some of the restraint force into the slab through the shear studs at their composite interface, potentially mitigating some of the reaction to the shear connection. During the natural fire's decay phase, the onset of residual tension will be impacted by the various modes of thermal damage or permanent deformation that developed during heating. More research is needed on the actual development of the push-pull nature of shear connection response in composite floor beams during heating and cooling under natural fire. Also, more research is needed to explore potential modifications that can be made to a shear connection to enhance its resistance to these fire-induced actions (Safari and Broujerdian, 2020; Selamet and Garlock, 2010).

Commentary on Two-Way Slab Contributions

It should be emphasized that the results presented in this paper focus solely on the one-way flexural response of composite filler floor beams under fire. Large-scale experimental testing on common steel framed floor assemblies with composite W-shaped filler beams at Cardington in the UK (Bailey et al., 1999; Wald et al., 2006), NIST in the United States (Choe et al., 2021a, 2021b) and elsewhere (Li et al., 2017; Selamet and Yolaçan, 2017; Wellman et al., 2011) have shown that the natural fire survivability of composite steel floor beams can be enhanced by engaging the composite slab in two-way tensile membrane and catenary action. The aforementioned ASCE exemplar report (ASCE, 2020) and other studies (Gernay and Khorasani, 2020; Huang et al., 2003; Jiang et al., 2014; Khorasani et al., 2019; Lamont et al., 2006, 2007; McAllister, 2014; Sanad et al., 2000) have also used 3D finite element (FE) numerical models of steel framed buildings with W-shape composite floor beams to demonstrate the beneficial contributions of two-way tensile membrane action in the composite slab when the elevated reactions in the slab and connections are taken into account. To unlock these benefits via PBSFD, however, the slab thickness and reinforcement must often be enhanced beyond what is conventionally used in current North American practice to achieve adequate load redistribution when

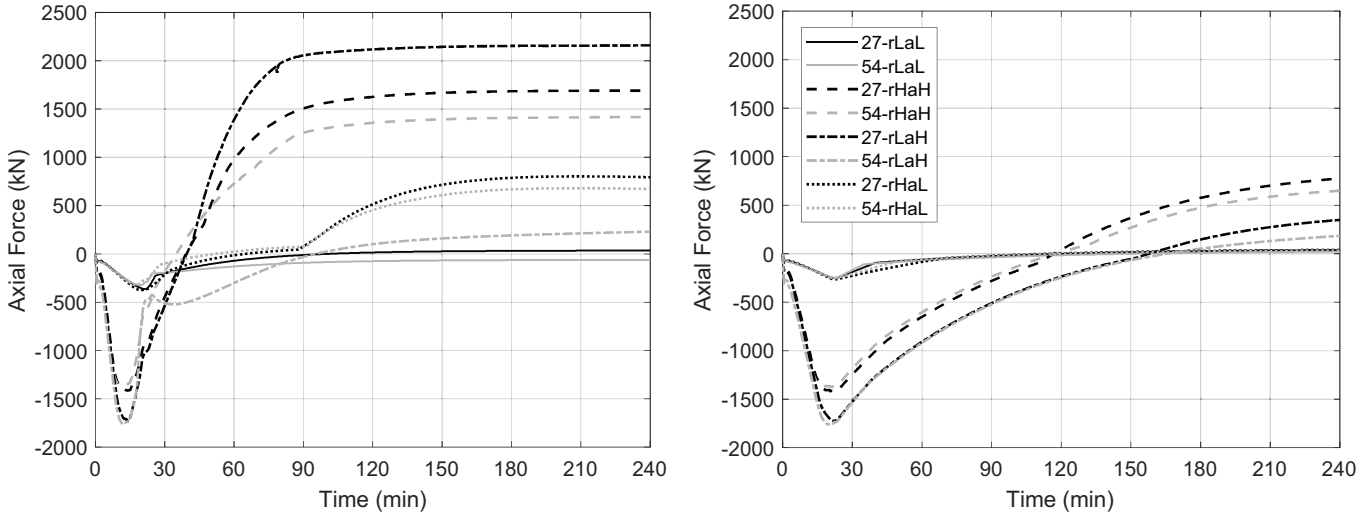

(a) P1 SFRM *(b) P2 SFRM*

Fig. 30. Beam end axial force for the W18×35 composite beam configurations under FH374 natural fire exposure with varying levels of SFRM (conversion note: 500 kN = 112.4 kips).

the filler beams develop large fire-induced deflections. Additionally, the aspect ratio of the floor system's bay dimensions and the relative fire resistance of beams and girders at the perimeter of each bay will play a role in the development of tensile slab contributions. Large deflections and catenary action will also increase the demand on the beam end connections. Tensile forces and increased rotation at high temperature would also need to be considered for connection design if the PBSFD performance objective relies on achieving large deflections.

The focus of this study on one-way flexural behavior for composite floor beams can still provide an efficient analytical alternative when the consideration of two-way slab action analysis may be cost prohibitive or impractical. The relationship for $T_{cr,BF}$ as a function of M/M_n per Table 1 would still provide a good prediction of the initial onset of rapid downward deflection for any fire-exposed W-shape floor beam assembly because tensile membrane and/or catenary effects would only be engaged once the beam achieves a significant amount of deflection. Any engagement of tensile slab effects would therefore provide a last resort for collapse prevention, though the structure would still be considered to be irreparably damaged if the relationship for $T_{cr,BF}$ as a function of M/M_n per Table 1 were exceeded.

CONCLUSIONS

Three realistically representative composite floor beam configurations (with different W-shape section sizes and one-way span lengths) were used for parametric numerical analysis, the matrix for which included the following: one standard fire curve and three natural fire curves, three levels of passive fire protection, realistic levels of axial and rotational restraint at the end of the beam to represent that provided by a shear connection, and varying levels of applied flexural loading. A previously validated heat transfer modeling approach was used for calculating steel temperatures for each flange and the web as individual lumped masses, and a one-dimensional FE heat transfer modeling approach was used to calculate the temperature gradient through the structural thickness of the floor slab. A previously validated fiber-beam FE structural modeling approach was used to model flexural response of the one-way composite beam assembly under fire. The following conclusions can be drawn based on the results of the parametric analyses:

- A deflection magnitude of $L^2/(400d_{beam})$ consistently indicated the loss of flexural resistance for exposure to any fire exposure in this study, regardless of parametric variation or composite beam configuration. This point also marks the onset of a catenary response in the beam end, which can only be supported if the beam end connections and the composite slab reinforcement have adequate capacity.
- The relationship in AISC 360-22, Table A-4.2.4, between moment retention factors and bottom flange temperature $T_{s,BF}$ can be reframed as a relationship between flexurally critical bottom flange temperature $T_{cr,BF}$ and the initially applied flexural utilization ratio M/M_n. This load-dependent representation of $T_{cr,BF}$ was also demonstrated as a reliably conservative indicator for the loss of flexural resistance for all composite beam model configurations under fire, again regardless of the level of applied fire protection, the level of beam end restraint, or the type of fire exposure.
- The relationship between midspan deflection and bottom flange temperature was relatively consistent across all beam configurations under all fire exposures in this study. These results suggest that $T_{s,BF}$ can be reliably used as an indicator of flexural response for one-way composite floor beams under fire. Specifically, the load-dependent values of $T_{cr,BF}$ based on AISC 360-22, Table A-4.2.4, can accurately signify the loss of flexural resistance under either standard or natural fire exposure. The application of various levels of axial and rotational restraint to the beam ends had a relatively marginal influence on the $T_{s,BF}$ at which the composite beam suffered a loss of flexural resistance at a given level of applied flexural loading.
- Variations in axial and rotational beam end restraint had more impact on the flexural response of these composite beam configurations when they were able to survive natural fire exposure thru burnout without flexural failure. Lower rotational stiffness at the beams ends produces increased deflection during the heating phase of a natural fire but less residual tensile force at the connections during cooling (due to less restraint of thermal expansion and therefore less permanent deformation during heating). Conversely, increased axial restraint initially provides a benefit to the composite floor assembly by reducing deflections during heating under natural fire but ultimately generates higher levels of residual tension in the connections during cooling (since the greater restraint of thermal expansion will have permanently shortened the beam during heating).
- Future work can extend the results of this study toward determining load-dependent values of $T_{s,BF}$ that correspond to varying levels of residual damage if the beam survives a natural fire through burnout. The residual reactions in the connections could also be quantified as a function of $T_{s,BF}$, initial M/M_n, and beam end restraint.

ACKNOWLEDGMENTS

Funding support for this project was provided by the American Institute of Steel Construction (AISC) via the Milek Faculty Fellowship (www.aisc.org/milek), of which Professor Quiel is the 2016 recipient. Additional funding to support Dr. Drury during his involvement in this research for his doctoral dissertation was provided by Lehigh University via a 2021 Faculty Innovation Grant. All opinions, findings, and conclusions expressed in this paper are the authors' and do not necessarily represent the policies and views of AISC or Lehigh University.

REFERENCES

AISC (2022), *Specification for Structural Steel Buildings*, ANSI/AISC 360-22, American Institute of Steel Construction, Chicago, Ill.

Alfawakhiri, F., Carter, C.J., Berhing, R.M., Zeeveld, P., Hervey, F.E., and Woods, L.C. (2016), "The Effects of Load Intensity and Restraint on the Fire Resistance of Steel and Composite Beams," *Proceedings of the 9th International Conference on Structures in Fire (SiF'16)*, Princeton University, Princeton, N.J.

ASCE (2020), *Performance-Based Structural Fire Design: Exemplar Designs of Four Regionally Diverse Buildings Using ASCE 7-16, Appendix E*, American Society of Civil Engineers, Reston, Va., https://doi.org/10.1061/9780784482698.

ASCE (2022), *Minimum Design Loads for Buildings and Other Structures*, ASCE/SEI 7-22, American Society of Civil Engineers, Reston, Va., https://doi.org/10.1061/9780784415788.

ASTM (2022a), *Standard Specification for Structural Steel Shapes*, ASTM A992/992M-22, ASTM International, West Conshohocken, Pa., https://doi.org/10.1520/A0992_A0992M-22.

ASTM (2022b), *Standard Specification for Steel Wire and Welded Wire Reinforcement, Plain and Deformed, for Concrete*, ASTM A1064-22, ASTM International, West Conshohocken, Pa., https://doi.org/10.1520/A1064_A1064M-22.

ASTM (2024), *Test Methods for Fire Tests of Building Construction and Materials*, ASTM E119-24, ASTM International, West Conshohocken, Pa., https://doi.org/10.1520/E0119-24.

Bailey, C.G., Lennon, T., and Moore, D.B. (1999), "The Behaviour of Full-Scale Steel-Framed Buildings Subjected to Compartment Fires," *The Structural Engineer*, Vol. 77, No. 8, pp. 15–21.

Bletzacker, R. (1967), "Fire Resistance of Protected Steel Beam Floor and Roof Assemblies as Affected by Structural Restraint," *Symposium on Fire Test Methods—Restraint & Smoke 1966*, ASTM International, West Conshohocken, Pa., https://doi.org/10.1520/STP41306S.

Block, F.M., Davison, J.B., Burgess, I.W., and Plank, R.J. (2013), "Principles of a Component-Based Connection Element for the Analysis of Steel Frames in Fire," *Engineering Structures*, Vol. 49, pp. 1,059–1,067, https://doi.org/10.1016/j.engstruct.2012.07.025.

Burgess, I.W., Davison, J.B., Dong, G., and Huang S.-S. (2012), "The Role of Connections in the Response of Steel Frames to Fire," *Structural Engineering International*, Vol. 22, No. 4, pp. 449–461, https://doi.org/10.2749/101686612X13363929517811.

Carino, N.J., Starnes, M.A., Gross, J.L., Yang, J.C., Kukuck, S.R., Prasad, K.R., and Bukowski, R.W. (2005), *Passive Fire Protection. Federal Building and Fire Safety Investigation of the World Trade Center Disaster*, NIST NCSTAR 1-6A, National Institute of Standards and Technology, Gaithersburg, Md., https://tsapps.nist.gov/publication/get_pdf.cfm?pub_id=101041.

Carter, C.J. and Alfawakhiri, F. (2013), "Restrained or Unrestrained?" *Modern Steel Construction*, September, https://www.aisc.org/globalassets/modern-steel/archives/2013/09/uld982.

CEN (2005), *Eurocode 3: Design of Steel Structures—Part 1-2: General Rules—Structural Fire Design*, EN 1993-1-2:2005, European Commission for Standardization, Brussels, Belgium.

CEN (2008a), *Eurocode 4: Design of Composite Steel and Concrete Structures—Part 1-2: General Rules—Structural Fire Design*, EN 1994-1-2:2005, European Commission for Standardization, Brussels, Belgium.

CEN (2008b), *Eurocode 2: Design of Concrete Structures—Part 1-2: General Rules—Structural Fire Design*, EN 1992-1-2:2004, European Commission for Standardization, Brussels, Belgium.

CEN (2009), *Eurocode 1: Actions on Structures—Part 1-2: General Actions—Actions on Structures Exposed to Fire*, EN 1991-1-2:2002, European Commission for Standardization, Brussels, Belgium.

Choe, L., Ramesh, S., Dai, X., Hoehler, M., and Bundy, M. (2021a), "Experimental Study on Fire Resistance of a Full-Scale Composite Floor Assembly in a Two-Story Steel Framed Building," *Journal of Structural Fire Engineering*, Vol. 13, No. 2, pp. 145–161, https://doi.org/10.1108/JSFE-05-2021-0030.

Choe, L., Ramesh, S., Grosshandler, W., Hoehler, M., Seif, M., Gross, J., and Bundy, M. (2020), "Behavior and Limit States of Long-Span Composite Floor Beams with Simple Shear Connections Subject to Compartment Fires: Experimental Evaluation," *Journal of Structural Engineering*, Vol. 146, No. 6, p. 04020088, https://doi.org/10.1061/(ASCE)ST.1943-541X.0002627.

Choe, L., Ramesh, S., Hoehler, M., Seif, M., Bundy, M., Reilly, J., and Glisic, B. (2019), *Compartment Fire Experiments on Long-Span Composite-Beams with Simple Shear Connections, Part 2: Test Results*, NIST TN 2055, National Institute of Standards and Technology, Gaithersburg, Md., https://doi.org/10.6028/NIST.TN.2055.

Choe, L., Ramesh, S., Zhang, C., and Clifton, C. (2021b), "Behavior of Composite Floor Assemblies Subject to Fire: Influence of Slab Reinforcement," *Ce/Papers*, Vol. 4, No. 2-4, pp. 1,353–1,360, https://doi.org/10.1002/cepa.1431.

Drury, M.M. (2022), *Critical Temperature Relationships for the Performance-Based Design of Realistically-Restrained Steel Composite Floor Assemblies*, Ph.D. Thesis, Lehigh University, Bethlehem, Pa.

Drury, M.M., Kordosky, A.N., and Quiel, S.E. (2020), "Structural Fire Resistance of Partially Restrained, Partially Composite Floor Beams, II: Modeling," *Journal of Constructional Steel Research*, Vol. 167, p. 105946, https://doi.org/10.1016/j.jcsr.2020.105946.

Drury, M.M., Kordosky, A.N., and Quiel, S.E. (2021), "Robustness of a Partially Restrained, Partially Composite Steel Floor Beam to Natural Fire Exposure: Novel Validation and Parametric Analysis," *Journal of Building Engineering*, Vol. 44, p. 102533, https://doi.org/10.1016/j.jobe.2021.102533.

Drury, M.M. and Quiel, S.E. (2023a), "Standard versus Natural Fire Resistance for Partially Restrained Composite Floor Beams: 1—Testing," *Journal of Constructional Steel Research*, Vol. 202, p. 107768, https://doi.org/10.1016/j.jcsr.2022.107768.

Drury, M.M. and Quiel, S.E. (2023b), "Standard versus Natural Fire Resistance for Partially Restrained Composite Floor Beams: 2—Analysis," *Journal of Constructional Steel Research*, Vol. 202, p. 107767, https://doi.org/10.1016/j.jcsr.2022.107767.

Drury, M.M. and Quiel, S.E. (2025), "Load-Dependent Critical Temperatures for Standard Fire Resistance of W-Shape Floor Beam Assemblies: Experimental Validation and Simplified Analysis," *Engineering Journal*, AISC, Vol. 62, No. 1, pp. 3–26, https://doi.org/10.62913/engj.v62i1.1335.

Dwaikat, M.M.S. and Kodur, V.K.R. (2011), "A Performance Based Methodology for Fire Design of Restrained Steel Beams," *Journal of Constructional Steel Research*, Vol. 67, No. 3, pp. 510–524, https://doi.org/10.1016/j.jcsr.2010.09.004.

Fischer, E.C., Chicchi, R., and Choe, L. (2021), "Review of Research on the Fire Behavior of Simple Shear Connections," *Fire Technology*, Vol. 57, No. 4, pp. 1,519–1,540, https://doi.org/10.1007/s10694-021-01105-1.

Fischer, E.C. and Varma, A.H. (2017), "Fire Resilience of Composite Beams with Simple Connections: Parametric Studies and Design," *Journal of Constructional Steel Research*, Vol. 128, pp. 119–135, https://doi.org/10.1016/j.jcsr.2016.08.004.

Franssen, J.-M., Cowez, B., and Gernay, T. (2014), "Effective Stress Method to Be Used in Beam Finite Elements to Take Local Instabilities into Account," *Fire Safety Science*, Vol. 11, pp. 544–557, https://doi.org/10.3801/IAFSS.FSS.11-544.

Franssen, J.-M. and Gernay, T. (2017), "Modeling Structures in Fire with SAFIR®: Theoretical Background and Capabilities," *Journal of Structural Fire Engineering*, Vol. 8, No. 3, pp. 300–323, https://doi.org/10.1108/JSFE-07-2016-0010.

Franssen, J.-M. and Gernay, T. (2019), *User's Manual for SAFIR 2019: A Computer Program for Analysis of Structures Subjected to Fire*, University of Liege, Liege, Belgium.

Gamble, W.L. (1989), "Predicting Protected Steel Member Fire Endurance Using Spread-Sheet Programs," *Fire Technology*, Vol. 25, No. 3, pp. 256–273, https://doi.org/10.1007/BF01039782.

Garlock, M.E. and Selamet, S. (2010), "Modeling and Behavior of Steel Plate Connections Subject to Various Fire Scenarios," *Journal of Structural Engineering*, Vol. 136, No. 7, pp. 897–906, https://doi.org/10.1061/(ASCE)ST.1943-541X.0000179.

Gernay, T. and Franssen, J.-M. (2012), "A Formulation of the Eurocode 2 Concrete Model at Elevated Temperature That Includes an Explicit Term for Transient Creep," *Fire Safety Journal*, Vol. 51, pp. 1–9, https://doi.org/10.1016/j.firesaf.2012.02.001.

Gernay, T. and Khorasani, N.E. (2020), "Recommendations for Performance-Based Fire Design of Composite Steel Buildings Using Computational Analysis," *Journal of Constructional Steel Research*, Vol. 166, p. 105906, https://doi.org/10.1016/j.jcsr.2019.105906.

Ghojel, J.I. and Wong, M.B. (2005), "Three-Sided Heating of I-Beams in Composite Construction Exposed to Fire," *Journal of Constructional Steel Research*, Vol. 61, No. 6, pp. 834–844, https://doi.org/10.1016/j.jcsr.2004.11.006.

Hantouche, E.G., Khatib, K.K.A., and Jabotian, H.V. (2020), "Design of Simple Steel Connections under Fire Temperatures," *Engineering Journal,* AISC, Vol. 57, No. 3, pp. 145–178, https://doi.org/10.62913/engj.v57i3.1168.

Harmathy, T.Z. (1965), "Effect of Moisture on the Fire Endurance of Building Elements," in A.F. Robertson, ed., *Moisture in Materials in Relation to Fire Tests*, ASTM International, West Conshohocken, Pa., https://doi.org/10.1520/STP48429S.

Huang, Z., Burgess, I.W., and Plank, R.J. (1999), "The Influence of Shear Connectors on the Behaviour of Composite Steel-Framed Buildings in Fire," *Journal of Constructional Steel Research*, Vol. 51, No. 3, pp. 219–237, https://doi.org/10.1016/S0143-974X(99)00028-0.

Huang, Z., Burgess, I.W., and Plank, R.J. (2003), "Modeling Membrane Action of Concrete Slabs in Composite Buildings in Fire. II: Validations," *Journal of Structural Engineering*, Vol. 129, No. 8, pp. 1103–1112, https://doi.org/10.1061/(ASCE)0733-9445(2003)129:8(1103).

ICC (2023), *2024 International Building Code*, International Code Council, Country Club Hills, Ill., ISBN: 978-1-959851-62-2.

ISO (2019), *ISO 834-11:2014 Fire Resistance Tests—Elements of Building Construction—Part 11: Specific Requirements for the Assessment of Fire Protection to Structural Steel Elements*, International Organization for Standardization, Geneva, Switzerland.

Isolatek International (2020), "CAFCO 300 Spray-Applied Fireproofing Technical Data Sheet C-TDS-05-20," available at: https://www.isolatek.com/wp-content/uploads/2020/05/CAFCO-300_C-TDS_05-20.pdf.

Jeanes, D.C. (1984), *Predicting Temperature Rise in Fire Protected Structural Steel Beams*, SFPE TR84-1, Society of Fire Protection Engineers, Boston, Mass.

Jiang, J., Usmani, A., and Li, G.-Q. (2014), "Modelling of Steel-Concrete Composite Structures in Fire Using OpenSees," *Advances in Structural Engineering*, Vol. 17, No. 2, pp. 249–264, https://doi.org/10.1260/1369-4332.17.2.249.

Jiang, S.-C., Ranzi, G., Chen, L.-Z., and Li, G.-Q. (2017), "Behaviour and Design of Composite Beams with Composite Slabs at Elevated Temperatures," *Advances in Structural Engineering*, Vol. 20, No. 10, pp. 1451–1465, https://doi.org/10.1177/1369433216682507.

Khorasani, N.E., Gardoni, P., and Garlock, M. (2015), "Probabilistic Fire Analysis: Material Models and Evaluation of Steel Structural Members," *Journal of Structural Engineering*, Vol. 141, No. 12, p. 04015050, https://doi.org/10.1061/(ASCE)ST.1943-541X.0001285.

Khorasani, N.E., Garlock, M., and Gardoni, P. (2014), "Fire Load: Survey Data, Recent Standards, and Probabilistic Models for Office Buildings," *Engineering Structures*, Vol. 58, pp. 152–165, https://doi.org/10.1016/j.engstruct.2013.07.042.

Khorasani, N.E., Gernay, T., and Fang, C. (2019), "Parametric Study for Performance-Based Fire Design of U.S. Prototype Composite Floor Systems," *Journal of Structural Engineering*, Vol. 145, No. 5, p. 04019030, https://doi.org/10.1061/(ASCE)ST.1943-541X.0002315.

Kishi, N., Hasan, R., Chen, W.F., and Goto, Y. (1997), "Study of Eurocode 3 Steel Connection Classification," *Engineering Structures*, Vol. 19, No. 9, pp. 772–779, https://doi.org/https://doi.org/10.1016/S0141-0296(96)00151-4.

Kodur, V., Aziz, E., and Dwaikat, M. (2013), "Evaluating Fire Resistance of Steel Girders in Bridges," *Journal of Bridge Engineering*, Vol. 18, No. 7, pp. 633–643, https://doi.org/10.1061/(ASCE)BE.1943-5592.0000412.

Kodur, V.K.R., Naser, M., Pakala, P., and Varma, A. (2013), "Modeling the Response of Composite Beam–Slab Assemblies Exposed to Fire," *Journal of Constructional Steel Research*, Vol. 80, pp. 163–173, https://doi.org/10.1016/j.jcsr.2012.09.005.

Kodur, V.K.R. and Shakya, A.M. (2013), "Effect of Temperature on Thermal Properties of Spray Applied Fire Resistive Materials," *Fire Safety Journal*, Vol. 61, pp. 314–323, https://doi.org/10.1016/j.firesaf.2013.09.011.

Kordosky, A.N., Drury, M.M., and Quiel, S.E. (2020), "Structural Fire Resistance of Partially Restrained, Partially Composite Floor Beams, I: Experiments," *Journal of Constructional Steel Research*, Vol. 167, p. 105945, https://doi.org/10.1016/j.jcsr.2020.105945.

LaMalva, K.J. (ed.). (2018), *Manual of Practice 138: Structural Fire Engineering*, American Society of Civil Engineers, Reston, Va., https://doi.org/10.1061/9780784415047.

LaMalva, K., Bisby, L., Gales, J., Gernay, T., Hantouche, E., Jones, C., Morovat, A., Solomon, R., and Torero, J. (2020), "Rectification of 'Restrained vs. Unrestrained,'" *Fire and Materials*, Vol. 44, No. 3, pp. 341–351, https://doi.org/10.1002/fam.2771.

Lamont, S., Gillie, M., and Usmani, A.S. (2007), "Composite Steel-Framed Structures in Fire with Protected and Unprotected Edge Beams," *Journal of Constructional Steel Research*, Vol. 63, No. 8, pp. 1,138–1,150, https://doi.org/10.1016/j.jcsr.2006.10.001.

Lamont, S., Lane, B., Flint, G., and Usmani, A. (2006), "Behavior of Structures in Fire and Real Design—A Case Study," *Journal of Fire Protection Engineering*, Vol. 16, No. 1, pp. 5–35, https://doi.org/10.1177/1042391506054038.

Li, G.-Q., Zhang, N., and Jiang, J. (2017), "Experimental Investigation on Thermal and Mechanical Behaviour of Composite Floors Exposed to Standard Fire," *Fire Safety Journal*, Vol. 89, pp. 63–76, https://doi.org/10.1016/j.firesaf.2017.02.009.

Lim, O.K., Choi, S., Kang, S., Kwon, M., and Choi, J.Y. (2020), "Fire Performance of Headed Shear Studs in Profiled Steel Sheeting," *Journal of Constructional Steel Research*, Vol. 164, p. 105791, https://doi.org/10.1016/j.jcsr.2019.105791.

Liu, J. and Astaneh-Asl, A. (2004), "Moment–Rotation Parameters for Composite Shear Tab Connections," *Journal of Structural Engineering*, Vol. 130, No. 9, pp. 1,371–1,380, https://doi.org/10.1061/(ASCE)0733-9445(2004)130:9(1371).

Martinez, J. and Jeffers, A.E. (2021), "Analysis of Restrained Composite Beams Exposed to Fire," *Engineering Structures*, Vol. 234, p. 111740, https://doi.org/10.1016/j.engstruct.2020.111740.

McAllister, T.P. (2014), "Sensitivity of Composite Floor System Response at Elevated Temperatures to Structural Features," *Engineering Structures*, Vol. 58, pp. 115–128, https://doi.org/10.1016/j.engstruct.2013.09.026.

Mirza, O. and Uy, B. (2009), "Behaviour of Headed Stud Shear Connectors for Composite Steel–Concrete Beams at Elevated Temperatures," *Journal of Constructional Steel Research*, Vol. 65, No. 3, pp. 662–674, https://doi.org/10.1016/j.jcsr.2008.03.008.

Moss, P.J., Buchanan, A.H., Seputro, J., Wastney, C., and Welsh, R. (2004), "Effect of Support Conditions on the Fire Behaviour of Steel and Composite Beams," *Fire and Materials*, Vol. 28, No. 2-4, pp. 159–175, https://doi.org/10.1002/fam.855.

Quiel, S. and Garlock, M. (2010), "Parameters for Modeling a High-Rise Steel Building Frame Subject to Fire," *Journal of Structural Fire Engineering*, Vol. 1, No. 2, pp. 115–134, https://doi.org/10.1260/2040-2317.1.2.115.

Rackauskaite, E., Kotsovinos, P., Jeffers, A., and Rein, G. (2019), "Computational Analysis of Thermal and Structural Failure Criteria of a Multi-Storey Steel Frame Exposed to Fire," *Engineering Structures*, Vol. 180, pp. 524–543, https://doi.org/10.1016/j.engstruct.2018.11.026.

Ramesh, S., Choe, L., Seif, M., Hoehler, M., Grosshandler, W., Sauca, A., Bundy, M., Luecke, W., Bao, Y., Klegseth, M., Chen, G., Reilly, J., and Glisic, B. (2019), *Compartment Fire Experiments on Long-Span Composite-Beams with Simple Shear Connections Part 1: Experimental Design and Beam Behavior at Ambient Temperature*, NIST TN 2054, National Institute of Standards and Technology, Gaithersburg, Md., https://doi.org/10.6028/NIST.TN.2054.

Sadek, F., El-Tawil, S., and Lew, H.S. (2008), "Robustness of Composite Floor Systems with Shear Connections: Modeling, Simulation, and Evaluation," *Journal of Structural Engineering*, Vol. 134, No. 11, pp. 1,717–1,725, https://doi.org/10.1061/(ASCE)0733-9445(2008)134:11(1717).

Safari, P. and Broujerdian, V. (2020), "Strategies to Increase the Survivability of Steel Connections in Fire," *Structures*, Vol. 28, pp. 2335–2354, https://doi.org/10.1016/j.istruc.2020.10.033.

Sanad, A.M., Rotter, J.M., Usmani, A.S., and O'Connor, M.A. (2000), "Composite Beams in Large Buildings under Fire—Numerical Modelling and Structural Behaviour," *Fire Safety Journal*, Vol. 35, No. 3, pp. 165–188, https://doi.org/10.1016/S0379-7112(00)00034-5.

Seif, M.S., Main, J.A., and McAllister, T.P. (2013), "Performance of Steel Shear Tab Connections at Elevated Temperatures," *Proceedings of the Annual Stability Conference*, April, St. Louis, Mo., https://www.aisc.org/globalassets/continuing-education/ssrc-proceedings/2013/performance-of-steel-shear-tab-connections-at-elevated-temperatures.pdf.

Selamet, S. and Garlock, M.E. (2010), "Robust Fire Design of Single Plate Shear Connections," *Engineering Structures*, Vol. 32, No. 8, pp. 2,367–2,378, https://doi.org/10.1016/j.engstruct.2010.04.011.

Selamet, S. and Yolaçan, T.F. (2017), "Steel Frame—Concrete Slab Composite Floor Fire Resistance Experiment," *Teknik Dergi*, Vol. 28, No. 3, pp. 8,007–8,022, https://eskisakarya.imo.org.tr/resimler/ekutuphane/pdf/17888_23_42.pdf.

Selden, K.L. (2014), *Structural Behavior and Design of Composite Beams Subjected to Fire*, Ph.D. Thesis, Purdue University, West Lafayette, Ind.

Selden, K.L., Fischer, E.C., and Varma, A.H. (2016a), "Experimental Investigation of Composite Beams with Shear Connections Subjected to Fire Loading," *Journal of Structural Engineering*, Vol. 142, No. 2, p. 04015118, https://doi.org/10.1061/(ASCE)ST.1943-541X.0001381.

Selden, K.L. and Varma, A.H. (2016b), "Composite Beams under Fire Loading: Numerical Modeling of Behavior," *Journal of Structural Fire Engineering*, Vol. 7, No. 2, pp. 142–157, https://doi.org/10.1108/JSFE-06-2016-011.

Selden, K.L. and Varma, A.H. (2016c), "Flexural Capacity of Composite Beams Subjected to Fire: Fiber-Based Models and Benchmarking," *Fire Technology*, Vol. 52, No. 4, pp. 995–1014, https://doi.org/10.1007/s10694-016-0565-7.

UL (2020), *UL 263: Standard for Fire Tests of Building Construction and Materials*, Underwriters Laboratories, Inc., Northbrook, Ill.

UL (2022a), *Fire Resistance Directory*, Underwriters Laboratories, Inc., Northbrook, Ill., http://productspec.ul.com/index.php.

UL (2022b), "BXUV.D902—Fire-Resistance Ratings—ANSI/UL 263: Design D902," Underwriters Laboratories, Inc., Northbrook, Ill., https://iq.ulprospector.com/en/profile?e=13878.

UL (2022c), "BXUV.D982—Fire-Resistance Ratings—ANSI/UL 263: Design D982," Underwriters Laboratories, Inc., Northbrook, Ill., https://iq.ulprospector.com/en/profile?e=13952.

Vinnakota, M.R., Foley, C.M., and Vinnakota, S. (1988), "Design of Partially or Fully Composite Beams with Ribbed Metal Deck Using LRFD Specifications," *Engineering Journal*, AISC, Vol. 25, No. 2, pp. 60–78, https://doi.org/10.62913/engj.v25i2.498.

Wald, F., Simões da Silva, L., Moore, D.B., Lennon, T., Chladná, M., Santiago, A., Beneš, M., and Borges, L. (2006), "Experimental Behaviour of a Steel Structure under Natural Fire," *Fire Safety Journal*, Vol. 41, No. 7, pp. 509–522, https://doi.org/10.1016/j.firesaf.2006.05.006.

Wang, A.J. (2012), "Numerical Investigation into Headed Shear Connectors under Fire," *Journal of Structural Engineering*, Vol. 138, No. 1, pp. 118–122, https://doi.org/10.1061/(ASCE)ST.1943-541X.0000428.

Wang, W., Engelhardt, M.D., Li, G., and Huang, G. (2017a), "Behavior of Steel–Concrete Partially Composite Beams Subjected to Fire—Part 1: Experimental Study," *Fire Technology*, Vol. 53, No. 3, pp. 1,039–1,058, https://doi.org/10.1007/s10694-016-0618-y.

Wang, W., Wang, K., Engelhardt, M.D., and Li, G. (2017b), "Behavior of Steel–Concrete Partially Composite Beams Subjected to Fire—Part 2: Analytical Study," *Fire Technology*, Vol. 53, No. 3, pp. 1,147–1,170, https://doi.org/10.1007/s10694-016-0624-0.

Wellman, E.I., Varma, A.H., Fike, R., and Kodur, V. (2011), "Experimental Evaluation of Thin Composite Floor Assemblies under Fire Loading," *Journal of Structural Engineering*, Vol. 137, No. 9, pp. 1,002–1,016, https://doi.org/10.1061/(ASCE)ST.1943-541X.0000451.

Yu, L. and Frank, K.H. (2009), "Shear Behavior of A325 and A490 High-Strength Bolts in Fire and Post-Fire," *Engineering Journal,* AISC, Vol. 46, No. 2, pp. 99–106, https://doi.org/10.62913/engj.v46i2.1226.

Zhao, B. and Kruppa, J. (1997), *Fire Resistance of Composite Slabs with Profiled Steel Sheet and of Composite Steel Concrete Beams, Part 2: Composite Beams Final Report*, Publications Office of the European Commission: Directorate-General for Research and Innovation, Luxembourg.